Running head: CAMBRIAN CARBONATE SEQUENCE BOUNDARY IN NW SCOTLAND

SABKHA FACIES AND THE PRESERVATION OF A FALLING-STAGE SYSTEMS TRACT AT THE SAUK II–III SUPERSEQUENCE BOUNDARY IN THE LATE CAMBRIAN EILEAN DUBH FORMATION, NW SCOTLAND

ROBERT J. RAINE[1], M. PAUL SMITH[2]

[1]Geological Survey of Northern Ireland, Dundonald House, Upper Newtownards Road, Belfast, BT4 3SB (e-mail: robertr@bgs.ac.uk).

[2]Oxford University Museum of Natural History, Parks Road, Oxford, OX1 3PW.

Key words: Sabkha, Durness, Cambrian, Sauk, Laurentia

ABSTRACT

The Durness Group of northwest Scotland represents a nearly one-kilometer-thick succession of mid-Cambrian to lower Middle Ordovician carbonates. These rocks crop out in a narrow belt along the foreland of the Caledonian orogen and within the Moine Thrust zone, stretching some 170 km from Loch Eriboll southwestwards to the Isle of Skye. The Cambrian parts of the succession represent deposition on a paleo-southeast-facing, low-latitude, passively subsiding continental margin, situated at around 20° S. Carbonate deposition in Scotland formed part of the extensive Great American Carbonate Bank. The Sauk II–III supersequence boundary occurs above an interval of thin, meter-scale shallowing-upward peritidal cycles containing intraclast dolorudstones, stromatolites, tepees, siliciclastic sand, and surface karst. Evidence of former evaporites in the succession comprises pseudomorphs of nodular and bedded anhydrite, crystal-shaped calcite-filled vugs representing growth of sulfate, dissolution breccias, and local halite casts. These features represent sabkha facies arranged into cycles that constitute a preserved falling-stage systems tract (FSST). The top of the FSST is marked by a pronounced karst surface of sandstone-filled fissures. The section preserves a rare snapshot of a seldom-preserved environment on the Cambrian Laurentian margin. Its preservation during a time of falling relative sea level under slow tectonic subsidence is discussed.

INTRODUCTION

In Scotland, Cambro-Ordovician rocks crop out in a narrow belt along the autochthonous Caledonian foreland (Hebridean terrane) and within the Moine Thrust zone, stretching some 170 km from Loch Eriboll

43 southwestwards to the Isle of Skye (Fig. 1A). This almost continuous belt is
44 rarely more than 10 km in width and is overlain to the east by allochthonous
45 metasediments of the Moine Supergroup.
46 Scotland's Laurentian passive margin formed following the breakup of
47 the supercontinent Pannotia and initiation of the Iapetus Ocean following rift–
48 drift transition at 600–580 Ma (Torsvik et al. 1996; Scotese 2009). Recent
49 studies suggest that the rifting was a two-stage process forming the Iapetus
50 Ocean between west Gondwana and Laurentia at 570 Ma, followed by
51 continued rifting between 540 and 535 Ma, when the Laurentian passive
52 margin *sensu stricto* formed (Cawood et al. 2001). Lower Cambrian to
53 Ordovician carbonate sediments were deposited extensively along the margin
54 of Laurentia and are recorded from southeastern USA, through maritime
55 Canada and Newfoundland, to North Greenland (a distance of several
56 thousand kilometers), forming part of the Great American Carbonate Bank
57 (Derby et al. 2012).
58 Available paleogeographic reconstructions indicate that Laurentia lay
59 between 30˚ N and 30˚ S, with Scotland at a paleolatitude of approximately
60 20˚ S (Cocks and Torsvik 2006). The Cambro-Ordovician succession in
61 northwest Scotland is remarkably similar to sections in western
62 Newfoundland, Spitsbergen, and Northeast Greenland, and the stratigraphy
63 correlates well across these areas (Swett and Smit 1972a, 1972b; Cowie
64 1974; Swett 1981; Wright and Knight 1995; Smith and Rasmussen 2008;
65 Morgan 2012; Raine and Smith 2012).
66 Evidence of former evaporites has previously been recorded from the
67 Ordovician Sangomore Formation of the Durness Group (Young 1979) and

68 briefly documented from the lower and middle Eilean Dubh Formation (Raine
69 and Smith 2012) (Fig. 2).

70 *The Sauk Megasequence*

71 Large-scale sedimentary sequences have long been recognized in the
72 Paleozoic rocks of North America (Sloss 1963). On the craton, the Sauk
73 Megasequence, which is the oldest of these, begins with Lower Cambrian
74 strata and rests unconformably upon Precambrian-age basement. The Sauk
75 Megasequence is interpreted as reflecting deposition following progressive
76 flooding of the Laurentian Craton during prolonged sea-level rise (Morgan
77 2012). It is subdivided into three smaller-scale (second-order) transgressive–
78 regressive cycles or supersequences (Sauk I–III) (Palmer 1981; Morgan
79 2012), with each cycle separated by eustatic lowering of sea level.

80 In Scotland, as elsewhere along the contiguous lower Paleozoic paleo-
81 margin, the Sauk strata can be divided into a lower siliciclastic unit and an
82 overlying carbonate succession (Swett and Smit 1972a, 1972b; Smith and
83 Rasmussen 2008). The Sauk Megasequence in northwest Scotland consists
84 of c. 1130 m of strata (the siliciclastic Ardvreck Group and the overlying
85 carbonates of the Durness Group) (Fig. 2) and records progressive flooding of
86 the Neoproterozoic and Archean rocks on the craton.

87 The lowest carbonates in the succession (the base of the Durness
88 Group) correspond to the base of the Sauk II Supersequence. The boundary
89 of this supersequence with the overlying Sauk III lies within the middle Eilean
90 Dubh Formation (Raine and Smith 2012) and is the subject of this study.

91 *Biostratigraphy*

No biostratigraphically useful fossils have been discovered from the Cambrian-age Ghrudaidh (63 m thick) and Eilean Dubh (> 133 m thick) formations other than at the base and top of the succession. The base is well dated by the occurrence of trilobites and the small shelly fossil *Salterella*. A single specimen of the trilobite *Olenellus* aff. *reticulatus* discovered in the basal bed of the Ghrudaidh Formation (Huselbee and Thomas 1998) gives a maximum age of *Bonnia–Olenellus* Zone for the base of the Durness Group. At the top of the Eilean Dubh Formation, conodont studies located the Cambro-Ordovician boundary in the uppermost part of the formation below the overlying Sailmhor Formation (Huselbee 1998; Huselbee and Thomas 1998). Stratigraphic control in the intervening sediments is entirely reliant on recognizing sequence stratigraphic boundaries and correlating them with better-dated successions from other parts of the Laurentian margin (Raine and Smith 2012).

METHODS

Three sections were logged through part of the Eilean Dubh Formation at Balnakeil Bay, near Durness, Highland region, NW Scotland (Fig. 1). Facies associations were recorded, and meter-scale shallowing-upward cycles numbered sequentially up section. The described sections include a 20-m-thick interval across what is interpreted to be the level of the Sauk II–III boundary (Figs. 2 and 3) and two additional sections of shorter thickness (c. 4.5 m thick), both around six meters in either direction along strike from the principal measured section. These two additional sections were measured across the thinnest cycles and most pronounced karst surfaces to show how the cycles and component facies associations varied laterally. Reference to

117 “the studied section” in this paper relate to the main studied section unless
118 otherwise stated. The rocks dip gently to the east and the studied interval at
119 Balnakeil Bay stretches from NC 3738 6858 (British National Grid), on the
120 edge of the Kyle of Durness to NC 3918 6851. It is the type section and
121 affords the best exposures of the middle and upper Eilean Dubh Formation.
122 The top of the Eilean Dubh Formation and its boundary with the overlying
123 Sailmhor Formation is seen farther to the east [NC 3783 6877]. The section
124 starts approximately 75 m above the base of the formation (although there are
125 strata missing) and spans the interval 38–58 m below the top of the formation.

126 **FACIES ASSOCIATIONS**

127 Four facies associations (FA) can be recognized in the studied interval (Fig. 3;
128 Table 1). They include: (FA1) intraclast dolorudstones, (FA2) microbialitic
129 dolostone, (FA3) ripple-laminated or planar-laminated dolostone, and (FA4)
130 siliciclastic siltstone and sandstone. In the carbonates, sedimentary structures
131 are well preserved in fine-grained dolomite, and there is little evidence of
132 stylolitization.

133 Twenty-four meter-scale cycles are recognized in the interval. Whilst
134 they are discussed fully later, reference to cycle number is useful in the
135 context of the facies descriptions as they can be easily tied to the sedimentary
136 log for the main section in Figure 3.

137 *Facies Association 1: Intraclast Dolorudstone*

138 **Description.**—Intraclast dolorudstones (flat-pebble conglomerates)
139 (Table 1) are a minor but distinctive part of the succession. They are recorded
140 at the base of meter-scale cycles, in channels and filling hollows on karst
141 surfaces.

Interpretation.—There is no evidence of ductile deformation shown by the clasts, suggesting that they were completely lithified before erosion. The intraclasts were probably derived from the supratidal zone, where the hardening and cementation of muds is common in sediment that lies above the influence of most tides. The supratidal laminites were likely eroded and redeposited during storm activity. Mud polygons and tepees are highly susceptible to erosion, and brecciation of these cemented crusts is a common feature of the upper intertidal to supratidal zone (Assereto and Kendall 1977). During storms, widespread flooding of the inner part of the tidal flats and subsequent transport of indurated crust debris into channels and other localized depressions occur (Davies 1970). Clasts can become vertically orientated via sliding, being pinned against larger clasts, by becoming wedged between other steeply orientated clasts, or through infilling steep-sided scours (Mount and Kidder 1993). Tidal channels are an important part of modern tidal flats. They are recorded, for example, on the arid tidal flats of the Arabian Gulf (0–15 m deep), but they are comparatively more common on Andros Island flats, where they are 0–3 m deep (Shinn 1983, 1986). However, they have rarely been described from Cambro-Ordovician tidal-flat carbonates (Waters et al. 1989, and references therein; Cloyd et al. 1990). The dolorudstones occurring at the bases of cycles and as thin channel-shaped bodies observed in the upper parts of cycles in the main studied section are not interpreted to be the basal lag of laterally migrated channels but to be the product of storm reworking of desiccated supratidal flats and subsequent deposition in shallow scours on the upper intertidal flats, or karst depressions following base-level rise.

Facies Association 2: Microbialitic Dolostone

Description.—Microbialite facies (Table 1) show four end members, namely columnar branching digitate stromatolites, crinkly microbial planar stromatolites, stromatolites encrusting erosional surfaces, and mottled microbialites resembling thrombolites (see Hofmann 1969 and Grey 1989 for stromatolite terminology used here). Mottled microbialites are observed in cycles 2, 3, and 4, and digitate stromatolites are common in the lower half of many cycles. Only isolated occurrences of planar stromatolites and "encrusting" stromatolites are seen.

Interpretation.—Conditions needed for the development of microbial mats in the present day are a low to moderately smooth gradient (0.8–0.1 m km^{-1}) and restricted tidal influx with well-defined tidal zonation (Logan et al. 1974). Mats at Hamelin Pool, Western Australia, form from the supratidal (2 m above prevailing low water level) to lower intertidal zone (c. 4 m depth). The precipitation of gypsum destroys all microbial structures in the upper 20–30 cm of the intertidal zone (Kendall and Skipwith 1968; Evans et al. 1969; Butler et al. 1982; Warren 2006). This, combined with metazoan grazing in the lower intertidal and shallow subtidal areas, limits the development of the microbial flat in areas subject to these processes (Gebelein 1976).

Digitate stromatolites dominate the biostromes in the studied section and in modern tidal-flat environments where stromatolites are accumulating, they are the principal form in the subtidal pond environment (Logan et al. 1974). The internal digitate structure of the biostrome occurs beneath oval surface patches of colloform mat, less than 0.5 m in diameter. Apart from these areas of surface mat, the biostromes are almost completely buried by

192 sediment (Hoffman 1976). Typically, well-laminated, columnar stromatolites
193 represent deposition in an agitated to protected, lower intertidal to shallow
194 subtidal environment. This interpretation is based upon similar morphological
195 forms presently forming around exposed headlands at Shark Bay, Western
196 Australia (Logan 1961; Logan et al. 1974; Jahnert and Collins 2012), where
197 they form in turbulent environments. The turbulence causes scour of originally
198 planar microbial mats, and the disrupted mats acts as new loci for further
199 microbial colonization (Aitken 1967; Logan 1961). In the Eilean Dubh
200 Formation, the repeated colonization of surfaces by the digitate stromatolites
201 supports multiple episodes of growth and exposure, supporting a lower
202 intertidal setting or a subtidal environment that is periodically exposed.
203 The planar microbial mats represent more protected environments, as
204 evidenced from their growth in the depression formed by karst in C-13. In
205 other occurrences (e.g., C-7) they likely represent the formation of mats on
206 tidal flats in the upper intertidal to lower supratidal zone (Logan 1961; Logan
207 et al. 1974; Janhert and Colins 2012). Encrusting stromatolites colonized
208 submerged karst surfaces, but the environment of deposition is not known.
209 Where the stromatolites have been altered, either by dolomitization or by
210 growth of evaporites, they have lost some of their primary texture and begin to
211 resemble thrombolites.
212 *Facies Association 3: Ripple-Laminated and Planar-Laminated Dolostone*
213 **Description.**— Ripple-laminated and planar-laminated dolostones
214 (Figs. 3 and 6; Table 1) are typically disrupted by desiccation features (cracks
215 and tepees). The planar-laminated dolostone in some cycles contains
216 pseudomorphed evaporites of gypsum and/or anhydrite and is locally

deformed due to growth of the evaporites or brecciated due to their dissolution.

Interpretation.— The depositional environment of this facies association is interpreted to be upper intertidal to supratidal based upon the fine-grained, pale dolomite, the millimeter- to sub-millimeter-scale lamination, the associated underlying intertidal lithofacies, the close association with evaporite pseudomorphs, and the sedimentary structures present.

The environmental interpretation of much of the parallel-laminated carbonate relies upon associated sedimentary structures, as parallel lamination can form in a variety of different environments and by a variety of different means. The ripples are dominantly wave generated, but some subordinate current ripples are noted. Most of the laminated sediments forming on modern tidal flats occur in the supratidal zone deposited by wind or storm activity (Hardie and Ginsburg 1977; Shinn 1983). Windblown dust collected in the tidal flats of the Arabian Gulf is typically 60% detrital dolomite c. 30 μm across and clay minerals; however, sediment is also deposited by storms and the highest spring tides (Shinn 1968).

Tepees form on indurated supratidal crusts, and formation is thought to involve either of the following: salt hydration; slow dehydration then wetting during spring tides and storms or thermal expansion and moisture swelling within desiccation cracks. Tepees have been studied and described by many workers (see Kendall and Warren 1987 for a summary). In the present day, tepees are forming in Shark Bay (Davies 1970) and the Arabian Gulf (Kendall and Skipwith 1968; Assereto and Kendall 1977; Evamy 1973). These tepees

form the edges of large polygons, which form networks in the intertidal zone (Handford et al. 1983; Kendall and Warren 1987; Lokier and Steuber 2009).

Tidal-flat sediment of both modern and ancient sediments is deposited as layers of sand-size mud pellets, and although they may be destroyed by dolomitization or compaction, the ripple lamination is typically still visible. The ripple lamination represents deposition of carbonate silt, with the mud deposited in the slack water of receding tides. Ripples may form in the supratidal zone (Shinn 1983), but horizontal laminations, with or without cross bedding are mostly restricted to supratidal and upper intertidal settings (Shinn 1983). The small size of the ripples and the lack of subtidal features suggest an intertidal to lower supratidal setting on carbonate tidal flats. The dominance of wavy bedding, with some muddy drapes, supports intertidal-flat deposition. Paleocurrent directions indicate both northwest–southeast and east–west directions.

Facies Association 4: Siliciclastic Siltstone and Sandstone

Description.—The facies association includes siltstones and sandstones (Table 1), which are dominated by siliciclastic material (Fig. 7) and are commonly associated with surface karst at cycle tops. Quartz sand is observed throughout the study section, although it is relatively rare in the rest of the Eilean Dubh Formation.

Interpretation.—The red and purple color of the siltstone beds suggests iron staining, resulting from oxidizing (possibly subaerial) conditions and the high sphericity and frosting of the sand grains incorporated in the bed indicates a possible eolian origin (Krinsley and Doornkamp 1973). The reddened siltstones that are associated with karst surfaces may be the result

of *in situ* subaerial weathering, or possibly remobilization of sediments during the successive flooding event. They are here interpreted to be equivalent to incipient paleosol horizons, and they locally grade laterally into breccia representing possible regolith.

The silt and finer sand would have been able to be carried by wind onto the carbonate flats, as happens today on the sabkhas of the Arabian Gulf (Shinn 1986). Larger grains may have migrated via saltation and traction onto the shelf by the progradation of dunes (ergs) and then reworked by tidal action ("eolo-marine" deposition *sensu* Fischer and Sarnthein 1988), and it is possible they may have formed the distal fingers of a siliciclastic wedge, similar to those described by Mount (1985). A lack of rooted vascular plants on the nearby Cambrian craton probably facilitated the non-uniformitarian generation of large volumes of sediment (Dalrymple et al. 1985).

In modern environments, ergs migrate into the ocean bordering the Saharan Desert and are concentrated in two broad belts between 20º N to 40º N and 20º S to 40º S (Wilson 1971). In the Cambrian, ergs have been documented from the Backbone Ranges Formation (Mackenzie Mountains, Canada) by MacNaughton et al. (1997) and from the Wonewoc Formation (Wisconsin and Minnesota, USA) by Dott et al. (1986) and Runkel et al. (1998). It is not known how extensive dune systems were on the Scottish part of the Laurentian margin.

EVIDENCE OF FORMER EVAPORITES

A number of textures and minerals in the succession represent evidence for the existence of evaporites. They are independent of facies association, albeit generally located in the upper parts of the cycles in ripple-laminated and

291 planar-laminated dolostone, but they also occur in the microbial boundstone
292 facies. Since they are interpreted to be an early diagenetic overprint, in most
293 instances they are considered separately. The classification and
294 morphological descrption for nodular and bedded anhydrite of Maiklem et al.
295 (1969) and Forkner (2010) are followed here.

296 *Crystal Vugs*

297 **Description.**—Crystal vugs are observed in FA2 (Fig. 8D) and FA3.
298 Beds and lenses are observed in which there are concentrations of largely
299 euhedral crystal vugs (Figs. 8 and 9). The section contains one bed
300 composed almost entirely of crystal vugs in C-5 (Figs. 8 and 9B–D), but vugs
301 are also locally present in the underlying beds of C-4 (Fig. 9A). In C-5 the bed
302 is laterally variable, and is locally brecciated and deformed, with laminated
303 dolostone clasts in a matrix of crystal-vug-rich dolostone (Fig. 8A). The vuggy
304 bed also displays soft-sediment deformation associated with these crystal
305 shapes (Fig. 8B). The proportion of vugs varies greatly, and the bed is locally
306 a highly vuggy dolostone caused by dissolution of the cement from numerous
307 crystal vugs (Fig. 8C). The crystal vug bed is irregular to lens shaped and is
308 overlain by a contorted bed (Fig. 8D).

309 Crystal vugs range in length from 1 to 8 mm, and typically show no
310 preferred orientation (Fig. 9). They are seen in microbial dolostones in C-4,
311 where they have grown within stromatolites (Fig. 9A). In C-5, where they are
312 more abundant, they compose up to c. 50% of the total rock volume of some
313 beds and are locally associated with silica nodules. In thin section the crystals
314 are seen to be filled by nonferroan, sparry calcite (Fig. 9B). The shape of the

crystals varies from barrel and keg shaped to tabular or acicular, and twinned in some cases (Figs. 9C and 9D).

Interpretation.—Although the crystals are possibly pseudomorphs of anhydrite (which resulted from the pseudomorphing of gypsum) the crystal morphology does also bear resemblance to gypsum crystals grown experimentally in bentonite muds (Cody 1976) and to those described by Kennard (1981) from the Upper Cambrian of the Georgina Basin, Central Australia, where single crystals of calcite were interpreted to represent pseudomorphed gypsum. The vugs in the Eilean Dubh Formation are also very similar in size and habit to calcite-replaced gypsum crystals recorded by Lucia (1961) from the Permian Tansill Formation, Texas.

Handford et al. (1982) described 2-mm-long gypsum crystals in recent microbial-mat facies on a coastal sabkha in Abu Dhabi. Landward of the mat facies gypsum mush occurs in a lower supratidal setting. This belt of gypsum mush extends inland for some 2.5 km and is up to 30 cm thick. In the mid-supratidal zone, anhydrite replaces subsurface gypsum mush and forms nodules and beds (Handford et al 1982). The crystal-shaped vugs from the interval studied in the Eilean Dubh Formation are interpreted as originally composed of sulfate crystals that grew in the sediment. Their abundance and style resembles the gypsum mush recorded from recent coastal sabkhas.

Nodular Pseudomorphs

Description.—Quartz nodules are observed at a height of 5.3 m in the section (C-5). They range up to 8 cm in diameter and up to 5 cm in thickness and display an ovoid shape, with an irregular, knobbly (“cauliflower”) – shaped margin (Fig. 10A). In hand specimen the majority of nodules comprise white,

massive quartz with a macrocell texture, surrounded by fine-grained dolostones with dispersed crystal pseudomorphs. Rare examples are observed in C-6 and C-11 of replacement via finely crystalline dolomite. The dolomite nodule observed in C-11 shows an original distorted nodular mosaic texture, highlighted by hematite-rich seams (Fig. 10B).

In thin section the nodules show a transition from chalcedony (lutecite) at the margin to megaquartz and minor nonferroan calcite in the center of the nodule (Fig. 10C). The lutecite is in most cases radially arranged, and the remainder of the nodules comprise void-filling megaquartz and calcite (Fig. 9C). In plane light the dusty margins of the quartz crystals preserve the “felted lath” texture (Fig.10D) and in crossed-polarized light the quartz crystals are seen to contain inclusions of highly birefringent anhydrite up to 90 μm in length. The successive inner parts of the nodule contain length-slow chalcedony (lutecite), which forms spherules, up to 1 mm in diameter. Silicified evaporate nodules with anhydrite inclusions and textures have also been recorded from other intervals in the Durness Group, at the base of the Eilean Dubh Formation (Raine and Smith 2012), and from the Floian (Early Ordovician) Sangomore Formation (Young 1979).

Interpretation.—Replacement of anhydrite nodules by silica is a relatively common phenomenon in the rock record, and many cases have been recorded (e.g., West 1964; Folk and Pittman 1971; Siedlecka 1972; Chowns and Elkins 1974; Siedlecka 1976; Tucker 1976a, 1976b; Milliken 1979; Radke and Mathis 1980; Arbey 1980; Friedman and Shukla 1980). Many anhydrite nodules are silicified in a multistage process that involves both replacement and void filling (West 1964; Chowns and Elkins 1974).

Anhydrite nodules and beds are commonplace in the middle and upper sabkha of the Arabian Gulf (Shinn 1983).

Bedded-Evaporite Pseudomorphs

Description.—Dolostone interpreted to be pseudomorphed bedded anhydrite (Fig. 11) is found in two cycles (C-5 and C-13) in the logged interval. The lower bed (C-5) (7–14 cm thick) shows a ptygmatically folded cross section and is composed of light gray dolomite showing contorted laminae. The shape of the bed is marked by orange cherts at its upper and lower boundary (Fig. 11A). In plan view these cherts locally form circular patterns (Fig. 11B), and the surface is rich in quartz sand. Higher in the section, C-13 contains a bed with the same textures as those in C-5 (Fig 11C). This bed is laterally continuous over several meters but grades into breccias, cemented by red chert, and several meters farther along strike from the measured section the bed is represented by a karst surface, with depressions filled by planar to digitate stromatolites.

Interpretation.—The shape of the contorted dolomite bed in C-5 is delineated by cherts above and below. The bed is ptygmatically folded, and this shape bears close similarity with bedded anhydrite documented from recent sabkha environments that show enterolithic (ptygmatic) folds (Kendall 1984). In thin section the cherts contain inclusions of anhydrite. The rings of chert on the upper surface of the dolostone bed show that the apex of the fold has been truncated and may represent erosion of the sabkha surface and exposure of the anhydrite at a Stokes surface. This is somewhat speculative, but deflation of the vadose zone in sabkha environments is a common occurrence (Warren 1991). The bed observed higher in the succession (C-13)

390 is also interpreted to be pseudomorphed anhydrite as it possesses an
391 identical texture and is laterally equivalent with collapse breccias.
392 *Surface Cubic and Crustose Casts and Molds*
393 **Description.**—Equant shapes were found at one horizon (C-6) in the
394 section (Fig. 12). They range in size from 0.3 to 2.0 cm and form casts of
395 single (Fig. 12A), and more rarely composite cubic crystal shapes (Figs. 12B
396 and 12C). The casts are observed to have three-dimensional relief on the
397 underside of bedding planes and are composed of the same lithology as the
398 bed itself. Some loose blocks of dolostone from C-6 show a mass of poorly
399 developed cubic casts forming an irregular crustose surface to the underside
400 of the bedding plane (Fig. 12D). The casts are associated with purple, fine-
401 grained laminae that display mud cracks and contain some quartz sand
402 grains.
403 **Interpretation.**—The casts are interpreted to be the sediment fill of
404 impressions of single halite crystals (Fig. 12A) and locally halite hopper
405 crystals (Figs. 12B and 12C). The occurrences most likely represent halite
406 precipitation by concentration of seawater in ephemeral pools (Warren 2006).
407 Halite itself is not recorded in the sediment of the studied interval, and these
408 examples are more likely to be the impressions of crystals that were overlain
409 by fine-grained carbonate mud. Halite crystals typically form in the modern
410 sabkha environment but are seldom preserved, due to their high solubility
411 (Handford 1981). The surface showing multiple halite casts (Fig. 12D) may
412 represent a halite crust, which is recorded from sabkha environments (Warren
413 2006, p. 152).
414 *Evaporite Dissolution Breccias*

Description.—Localized beds of brecciated dolostone are associated with the evaporite pseudomorphs and differ from the intraclast rudstones in their association with pseudomorphs, clast shape, and bed geometry. Examples of both packbreccia (clast supported) and floatbreccia (clasts float in a finer matrix of granules, sand or mud) are observed (Fig. 13). Packbreccias can be further classified (Morrow 1982) into crackle (fitted clasts), mosaic (mildly disorientated), and rubble breccias (totally independent). The breccias from the studied section are all monomict and include mosaic packbreccias (Fig. 13 A), but most examples are crackle to mosaic packbreccias (Figs. 13B and C). There is one example of a floatbreccia (Fig. 13D). The lithic fragments in the breccias are similar to the rocks surrounding the breccia (dolomicrite), with the clasts locally showing a fitted texture. The spaces between the clasts are largely filled with cements, which are dominated by dolomite or chert. There is no indication of weathering, and the clasts are angular to subangular. Clast size varies from 0.4 cm to 6.0 cm. No imbrication, alignment, or grading is observed. The overall shape of the breccia body varies from tabular (Fig. 13C) to lenticular (Fig. 13D) (concordant) or irregular (Fig. 13A). Some of the breccias show a flat base and an irregular upper boundary (Fig. 13D).

Interpretation.—The breccias are interpreted to have formed by the dissolution of evaporites as they fulfil many of the criteria outlined by Beales and Oldershaw (1969), including flat base and irregular top, varied clast size, monomict composition, and association with supratidal facies in a succession containing pseudomorphs. Bed dissolution, as well as nodule and crystal replacement, can be syndepositional and driven by active phreatic flow or can

occur later, driven by compactional and thermobaric flushing (Warren 2006, p. 458). One bed in the section studied (in C-13) suggests that dissolution of the evaporites was syndepositional. In this bed, pseudomorphed anhydrite grades laterally into breccia facies and then farther along strike is represented by a karst surface filled by stromatolites.

During dissolution, if the cavity is only a few millimeters or centimeters high, the overburden founders gradually and gently, and so clast orientation is "fitted" and little disturbed by the process of dissolution; crackle and mosaic packbreccias will be commonplace (Warren 2006), as is the case in the Eilean Dubh Formation. The majority of breccias are of limited lateral extent and are associated with beds of nodular pseudomorphs. They likely represent dissolution of isolated nodules. If large local cavities develop, the collapse is more likely to produce disturbed rubble packbreccias. Clast-supported packbreccias result from dissolution of pure evaporites that are interbedded with indurated dolomites and other non-evaporite strata. In contrast, evaporite sequences interbedded with or underlying non-consolidated sediments, or evaporites with a high content of dispersed impurities, tend to produce matrix-supported floatbreccias (Warren 2006, p. 475). The single floatbreccia observed here is along strike from beds which are interpreted to be pseudomorphed, bedded anhydrite, suggesting that anhydrite either dissolved before lithification of the overlying sediment or that the single bed of anhydrite graded laterally into composite beds comprising intervening dolostone.

DISCUSSION

Development of Meter-Scale Shallowing-Upward Cycles in the Middle Eilean Dubh Formation

The majority of the Durness Group carbonates are arranged into meter-scale shallowing-upward cycles (Raine and Smith 2012). For the most part these are asymmetrical and conform to the definition of parasequences as described by Van Wagoner et al. (1990). Parasequences are defined as relatively conformable successions of genetically related beds or bedsets bounded by marine flooding surfaces (Van Wagoner et al. 1990). In the section described here, 24 cycles are recognized (C-1 to C-24) (Fig. 3). In the middle of the main measured section, their tops are marked by karstic surfaces, and so they are not parasequences in the strict sense, but are better termed cycles, equivalent to fourth- or fifth-order sequences of various authors (see Schlager 2004 for a summary). In other Cambrian Laurentian successions average cycle duration of 30,000 to 150,000 years has been calculated (Koerschner and Read 1989; Montañez and Osleger 1996).

At the tops of these high-order cycles in the middle Eilean Dubh Formation, surface karst takes the form of decimeter-scale scalloped surfaces (kaminitzas) (Fig. 14A), pinnacles, mounds, and solution-enlarged fractures (grikes) (Figs. 14B and 14D). The karst may be related either to solution resulting from exposure of cemented carbonates or to collapse following evaporite dissolution, with removal of the roof material over time. Shallow scallops formed by karstification then appear to have acted as ponds in which microbial mats formed (Fig. 14A); other surfaces dominated by enlarged fissures up to 30 cm deep occur, and these contain quartz sandstone with dolostone intraclasts (Fig. 14B). Locally, a few cycle boundaries appear to be separated by a rubbly conglomerate, which may represent a regolith (Fig. 14C). Large pinnacles and mounds in the studied succession are locally

490 flanked by coarser-grained conglomerates, attesting to their synoptic relief
491 during deposition of the overlying cycle (Fig. 14D). Beds below one of the
492 surface karsts display large cavities containing coarse pink calcite spar (Fig.
493 14E) that may represent a cement-filled example of subsurface karst.
494 This surface paleokarst is interpreted to have developed on bare
495 carbonate rock under prolonged subaerial conditions in the supratidal and/or
496 intertidal environment. Solution pans and enlarged fractures are a common
497 feature of supratidal environments of modern tropical and subtropical marine
498 coasts (Sweeting 1972), and on carbonates subaerially exposed in the
499 intertidal zone (Kaye 1959; Schneider 1976). There is a general transition
500 from deeply pitted and scalloped coastal limestones seaward into planated
501 tidal terraces (Kaye 1959). Read and Grover (1977) showed that subaerial
502 karst surfaces form more slowly than those in tidal settings. Karst in the
503 studied succession is similar to that described from the Middle Ordovician of
504 Virginia (Read and Grover 1977) and from time-equivalent strata of the Port
505 au Port Group (Campbells and Felix Members of the Petit Jardin Formation),
506 western Newfoundland (Chow and James 1992).
507 The thickness and facies evolution of a cycle depend on three
508 parameters that determine water depth: sediment accumulation rate,
509 subsidence rate, and the rate of eustatic sea-level change. There are a
510 number of models for creating cycles autocyclicly (Ginsburg 1971, Matti and
511 McKee 1976; Mossop 1979). In these models, sediment moves landward and
512 causes tidal flats to prograde, decreasing the carbonate factory and slowing
513 production. This then is eventually overcome by subsidence that rapidly floods
514 the flat, to create a new source area. Pratt and James (1986) proposed that

515 this happened on a number of prograding islands for the Lower Ordovician of
516 western Newfoundland, and Cloyd et al. (1990) invoked the lateral migration
517 of channels to form upward-shallowing peritidal cycles in Cambrian strata
518 from the central Appalachians. Although these processes certainly operate on
519 tidal flats, the extensive nature of many peritidal cycles does not support the
520 model offered by Pratt and James (1986) in most cases. Shinn et al. (1969)
521 showed that sediment can be eroded at one site and accumulate at the same
522 time farther along the shore. The autocyclic model cannot account for subtidal
523 cycles, but may contribute to the internal architecture (Osleger 1991). The
524 cause of these high-order cycles in the studied section is not known, but they
525 decrease in thickness and increase in the intensity of karst through the
526 interval, suggesting an allocyclic control.
527 The subsidence rates on passive margins are too low to drown
528 platform sediments in a reasonable period of time (Grotzinger 1986; Read
529 1989). The extent of cycles would seem to support a eustatic control, and
530 cycles from the Proterozoic and Cambrian have been shown to be
531 correlatable over kilometers to hundreds of kilometers (Markello and Read
532 1991; Grotzinger 1986; Read 1989). Therefore, cycles seen in Cambrian
533 carbonates principally represent shelf-wide events. Cycles recording
534 overprinting of depositional environments or widespread subaerial erosion are
535 attributed to be allocyclic (Grotzinger 1986) and driven by factors external to
536 the depositional system. They are mostly attributed to glacio-eustatic sea-
537 level fluctuations caused by climate cyclicity and fluctuations in glacial ice
538 volume. It is one of the few causes identified that can operate on this higher
539 frequency (Grotzinger 1986; Read 1989; Goldhammer et al. 1993) and

superimposed orders of eustatic sea-level oscillations (composite eustasy, Goldhammer et al. 1990) provide one of the best explanations for the upward shallowing of individual cycles, stacking patterns with cyclic successions, and the development of peritidal and subtidal cycles across the platform (Osleger and Read 1991).

If cycles are related to glacio-eustatic effects, then they must have involved low ice volumes associated with small-scale continental or alpine glaciations, because of the low amplitudes involved (Read 1989). This would be compatible with the view that the Cambrian recorded global greenhouse conditions (Crowley and Berner 2001; Miller et al. 2005). Eustatic changes from fluctuations in ice volume and geoidal effects could be both asymmetrical and small enough to generate cycles on the interpreted timescale (Grotzinger 1986).

Expression of the Sauk II–III Boundary Across Laurentia

Palmer (1960) postulated that, during the Cambrian, exposed Precambrian shield areas of Laurentia were surrounded by an inner detrital belt comprising shallow-marine siliciclastic sediments derived from the land areas, a middle carbonate belt, and outer shale deposits that accumulated beyond this belt. The boundaries between these belts shifted in response to changes in relative sea level and corresponding changes in the seaward dispersal of siliciclastic detritus (Runkel et al. 2007). The inner detrital belt was extensive along the southern Laurentian paleomargin (present-day eastern North America) in a number of epeiric seas, but thins towards the southeastern paleomargin (western Newfoundland, northwest Scotland and Northeast Greenland).

565 The Sauk II–III boundary has been recorded from many localities along
566 the Laurentian margin (Morgan 2012). It has its most pronounced sedimentary
567 expression in the more craton-ward sections and is frequently represented by
568 an influx of siliciclastic sediment into an otherwise carbonate-dominated
569 succession (Saltzman et al. 2004). Siliciclastic sediments were transported by
570 eolian processes onto the shelf during emergence and incorporated into cycle
571 caps or reworked by the successive marine transgression into the basal lag of
572 the next cycle (Read 1989; Koerschner and Read 1989; Cowan and James
573 1993). The Sauk II–III boundary is dated by trilobites to the Laurentian mid-
574 Steptoean Stage (*Dunderbergia* trilobite zone, equivalent to a middle Pabian –
575 lower Furongian age), and appears to mark maximum regression on the North
576 American craton (Palmer 1981; Taylor et al. 2009).
577 The Sauk II–III boundary is recognized in Arizona in the Abrigo
578 Formation, where shoreface facies representing the transgression of the Sauk
579 III overlie the boundary and locally constitute a FSST. In one section the
580 boundary is a pebble lag, but in others it is more cryptic because facies below
581 and above are sedimentologically similar (Łabaj and Pratt 2016). In northern
582 Utah, the Worm Creek Quartzite Member of the St. Charles Formation
583 coarsens up in the lower half into shoreface sands that represent the
584 boundary interval (Miller et al. 2003; Saltzman et al. 2004).
585 The Sauk II–III transition in eastern Tennessee spans the conformable
586 lithostratigraphic boundary between the Maynardville Formation and the
587 overlying Copper Ridge Dolomite (Glumac and Walker 1998, 2000). The
588 interval records exposure surfaces and quartz sand. Some of the cycles are
589 capped by subaerial exposure surfaces with up to 30 cm of erosional relief.

590 Evaporite molds and desiccation cracks are common in some of the
591 lithofacies.
592 The Felix Member (Berry Head Formation), western Newfoundland,
593 contains medium- to coarse-grained, frosted and well-rounded quartz sand in
594 millimeter-thick stringers, and there is a meter-thick quartz sandstone that is
595 interpreted to contain the Sauk II–III boundary (James et al. 1989; Westrop
596 1992; Cowan and James 1993; Saltzman et al. 2004).
597 The Sauk II–III boundary is present in the Wonewoc Sandstone (c. 40
598 m thick) in the Minnesota and Wisconsin areas, and comprises a lag of
599 coarse- to very coarse-grained sandstone one meter thick that contains small
600 pebbles of vein quartz and pink and white quartzite (Runkel et al. 1998). The
601 boundary merges into a correlative conformity in the central Iowa part of the
602 Upper Mississippi Valley epeiric ramp (Runkel et al. 1998, 2007; Saltzman et
603 al. 2004). Dott et al. (1986) recognized the eolian nature of parts of the
604 cratonic sand sheet, and documented ergs passing into eolian and fluvial
605 sand sheets.
606 The Sauk II –III boundary in the central Appalachians can be traced
607 from the Nittany Arch in Pennsylvania to the Great Valley in Maryland (Taylor
608 et al. 2009). In the inner detrital belt, the Lower Sandy Member (Gatesburg
609 Formation) is interpreted to equate to the Sauk II–III boundary, and in the
610 carbonate-dominated outer shelf in Maryland the Big Spring Station Member
611 (Conococheague Formation) comprises a condensed package, 75 m thick, of
612 dolomite and quartzarenite that correlate with the shallow facies in the
613 Gatesburg Formation. Taylor et al (2009) interpreted the Big Spring Station
614 Member to be a thick SBZ, but Brezinski et al. (2012) placed the Sauk II–III

615 boundary at the base. Previously the Sauk II–III boundary was placed in the
616 middle of the Big Spring Station Member (Palmer 1971a; Read 1989), but
617 data presented by Brezinski et al. 2012 suggest that the trilobites on which
618 this assertion was based came from the underlying Elbrook Formation. The
619 Big Spring Station Member has yielded no age diagnostic fauna. It is often
620 difficult to recognize sequence boundaries in siliciclastic sediments because
621 the depositional setting was not conducive to the development of features
622 diagnostic of subaerial exposure (Runkel et al 1998).
623 During regression on a carbonate margin, clastic sediment is
624 sometimes carried across the shelf and deposited at the toe of slope (Hunt
625 and Tucker 1992). In Sauk II–III coeval platform-margin deposits, such as the
626 Cow Head Group, western Newfoundland, the regression is represented by a
627 quartzose calcarenite sediment apron, deposited during a period of arrested
628 shallow-water sedimentation, eolian sand bypassing, and margin progradation
629 (James and Stevens 1986; James et al. 1989). Slope and shelf-margin facies
630 in eastern New York and Vermont contain periplatform breccias, and
631 resedimented and locally channelized quartz sands (Read 1989). In Maryland,
632 the Sauk II–III boundary in the Conococheague Formation correlates with
633 lowstand deposits of limestone conglomerate interbedded with sandy
634 grainstone and dark shale, submarine-fan complex of the Frederick Formation
635 (Brezinski 2004). The deposition of basin-floor fans and megabreccias,
636 resulting from slope bypass, is not necessarily an indication of regression and
637 erosion on the platform, since Hunt and Tucker (1992) pointed out that
638 erosion of carbonates is typically chemical. However, during a lowstand,
639 collapse of the exposed carbonate margin or the shoulder of distally

640 steepened ramps may take place, resulting in deposition of megabreccia in a
641 toe-of-slope apron (Hunt and Tucker 1992).

642 *Causes and Scale of the Sauk II–III Boundary*

643 The Sauk II–III supersequence boundary was originally described as a
644 disconformity or paraconformity that separates Dresbachian from Franconian
645 strata at several places in North America (Lochman-Balk 1971; Palmer 1971a,
646 1971b, 1981), and the successions in cratonic settings are normally missing
647 the *Dunderbergia* Zone (Palmer 1981). The Sauk II–III boundary interval is
648 interpreted to mark a pronounced sea-level fall then rise lasting 3.6 million
649 years (Saltzman et al. 2004).

650 The Laurentian Sauk II–III boundary corresponds with the peak of the
651 Steptoean positive carbon isotope excursion (SPICE) in many sections across
652 the paleocontinent (Glumac and Walker 1998; Saltzman et al. 1998, 2000,
653 2004). The SPICE event has also been recorded from time-equivalent strata
654 in China, Kazakhstan, Australia (Saltzman et al. 2000, 2004), Argentina (Sial
655 et al. 2008, 2013), the U.K. (Woods et al. 2011), Siberia (Kouchinsky et al.
656 2008), and Sweden (Ahlberg et al. 2009). Despite this evidence for a global
657 perturbation in the carbon cycle, the precise cause of the SPICE event and its
658 connection with sea-level change at the Sauk II–III boundary is not yet fully
659 understood.

660 In Laurentian sections there are examples where the transition from
661 Sauk II to Sauk III represents a clear sequence boundary (Saltzman et al.
662 2004; Runkel et al. 2007), but the scale and significance of this boundary has
663 been questioned (Chow and James 1987; Cowan and James 1993), and in
664 many cases the boundary is cryptic, lying within a sandstone unit without a

665 marked exposure surface. In the Upper Mississippi Valley where a subaerial
666 unconformity is recognized in the Wonewoc Sandstone, Runkel et al. (1998)
667 used facies relationships across six states to estimate a shoreline regression
668 of about 300 km, corresponding to a fall of a few tens of meters from an
669 inferred shelf gradient of 0.1 m/km.
670 Osleger and Read (1993) correlated the Sauk II–III boundary between
671 basins across the U.S. and considered it to be a Type 1 sequence boundary,
672 but noted that this was expressed as “transitional zones” of stacked thin
673 cycles composed of restricted lithofacies exhibiting evidence for intermittent
674 exposure. Glumac and Walker (2000) also referred to the Sauk II–III transition
675 as a sequence-boundary zone (as defined by Montañez and Osleger 1993).
676 In the Felix Member, western Newfoundland, Chow and James (1987) placed
677 a sequence boundary in the interval containing quartz sand and showing a
678 biostratigraphically “condensed” section of trilobite zones (equating to the
679 Sauk II–III boundary interval); they did not consider it to represent a significant
680 sequence boundary because it lay within their larger scale grand cycles.
681 Cowan and James (1993) recorded the presence of the same interval of
682 quartz sand and also recorded evaporite pseudomorphs in their “desiccated
683 laminite” fining-upwards cycles, but they did not place the sequence boundary
684 within this facies, and instead placed it at the boundary between “ribbon rock”
685 and bioherm cycles.
686 *Expression of the Sauk II–III Supersequence Boundary in the Middle Eilean*
687 *Dubh Formation*
688 In the Durness Group, siliciclastic material represents a minor constituent of
689 the succession. Quartz sandstone is present only as thin beds within a largely

690 dolostone sequence, but the entire interval is characterized by dispersed
691 medium- to lower very coarse-grained quartz grains (Figs. 3 and 15). Thin
692 sandstone beds cap many of the meter-scale cycles, occurring as lenses and
693 stringers or filling the hollows of irregular, scalloped and karstified cycle tops
694 (Fig. 3). The interval is also marked by abundant intraclast dolorudstones,
695 tepee structures, and evaporite pseudomorphs of gypsum and/or anhydrite
696 (Fig. 3) and locally halite. Overall, this interval marks a major shallowing of
697 facies and compares well with other sections across Laurentia that show
698 shallowing of facies associated with increased siliciclastic sediment input at
699 the Sauk II–III boundary.

700 *Development of a Sabkha Associated with the Sauk II–III Supersequence*
701 *Boundary in the Middle Eilean Dubh Formation*

702 Tidal flats are protected from waves, and are separated from the open ocean
703 by a wide, shallow shelf lagoon, by barrier islands, or because they lie in
704 restricted embayments (Hardie 1986). In modern peritidal settings, landward
705 of the intertidal flats, a supratidal marsh often develops in humid climates,
706 such as in the Bahamas, but in more arid settings such as the Arabian Gulf, a
707 coastal sabkha commonly develops (Shinn 1983). Sulfates, predominantly
708 gypsum and anhydrite, form on humid tidal flats during the dry season but
709 disappear during the wet season and therefore are rarely preserved (Shinn
710 1983). In the Arabian Gulf, where the annual rainfall is less than 40 mm,
711 evaporites are much more common and include sulfates and minor halite
712 (Alsharhan and Kendall 2003). Early dolomite is common in sabkha
713 environments (Patterson and Kinsman 1982), and quartz sand is a common
714 feature of the sabkhas in the Arabian Gulf, especially along the shore of Qatar

715 (Shinn 1986), where medium to coarse sand has spilled into the Gulf to
716 produce a quartz sand sabkha. Barchan dunes, 20–30 m high, march across
717 the flats and spill into the sea, producing marine sediments but having an
718 eolian origin (Shinn 1986).
719 The supratidal environment experiences large fluctuations in salinity,
720 and therefore bioturbation and grazing is limited and microbial mats thrive.
721 These mats may extend down into the upper intertidal zone in arid
722 environments (Shinn 1986). Desiccation cracks are also diagnostic of the
723 supratidal zone, as are tepees, evaporite pseudomorphs, and evaporite
724 dissolution breccias (Hardie 1977; Shinn 1983, 1986).
725 Sabkhas are exposed to the effects of wind and sun for much of the
726 time but are occasionally flooded by meteoric freshwaters and saline marine
727 storm waters. The combination of different depositional and diagenetic
728 conditions results in an assemblage of sediments and diagenetic minerals
729 (particularly anhydrite) that characterize a sabkha. The best-documented
730 modern examples of sabkha sedimentation occur around the shores of the
731 Arabian Gulf (Evans et al. 1969; Kendall and Skipwith 1969; Purser 1973;
732 Kendall 1984; Alsharhan and Kendall 1994, 2003; Al-Farraj 2005). The
733 supratidal portion of the sabkha can be divided into three subzones, (lower,
734 middle, and upper) (Table 2) with distinct physical characteristics (Patterson
735 and Kinsman 1981; Butler et al. 1982).
736 The preservation potential of sabkhas appears to have been low on
737 Cambrian shelves in Laurentia, or they have gone largely unrecorded in the
738 Cambrian rock record. Few sabkhas of this age have been recorded, and
739 Handford (1981) in his review and classification of sabkhas did not record any

740 Cambrian examples, although a paper by Laughrey (1994) describes a
741 shallowing-upward succession of dolostones from a core in the Ore Hill
742 Member of the Gatesburg Formation, Pennsylvania. The interval passes
743 upward from oolitic, fossiliferous dolostone to laminated anhydrite, dolostone
744 and stromatolites, to nodular anhydrites. The succession is sharply overlain
745 by burrow-mottled subtidal dolostones. This interval represents sediments of
746 the lower parts of the Sauk III supersequence. Examples of sabkha facies are
747 also known from the Lower Ordovician Jefferson City and Cotter dolomites of
748 southern Missouri (Overstreet et al. 2003). Features include quartz-replaced
749 anhydrite nodules, quartz sand in cycles, subaerial exposure features such as
750 desiccation cracks, small-scale tepees, and silicified solution collapse
751 breccias. Hopper halite molds and ghosts of gypsum laths are recorded at
752 cycle tops (Overstreet et al. 2003).
753 A few ancient carbonate platform sequences contain evidence of
754 dolomitization and anhydrite-nodule development in the subtidal and intertidal
755 facies, and have therefore been interpreted as sabkhas, but they lack the
756 overlying supratidal sabkha (Warren and Kendall 1985). There is a delicate
757 balance between deflation of the sabkha surface and the position of the water
758 table. In Upper Cambrian strata across the Appalachians there is a paucity
759 (with the exception of the subsurface Gatesburg Formation documented by
760 Laughrey 1994) of examples of bedded evaporites or pseudomorphs and
761 dissolution breccias, and only isolated silicified nodules are present. The
762 planar erosional surfaces at the cycle tops in the Appalachians were
763 suggested to result from the removal of sediment at a deflation surface
764 (Osleger and Read 1991).

765 The presence of nodular anhydrite does not necessarily suggest a
766 sabkha in itself. Three components must be present for a sabkha to be
767 securely identified: a) subtidal, intertidal, and supratidal sediments that
768 incorporate laminated microbial mats; b) a supratidal unit that contains
769 evidence of sulfate precipitation; and c) an erosion surface capping the
770 succession (Warren and Kendall 1985). The cycles underlying the Sauk II–III
771 boundary in the Eilean Dubh Formation contain all three of these components
772 and allow a sabkha origin to be confidently interpreted. Shallowing-upwards
773 cycles C-5 – C-14 exhibit evaporite pseudomorphs, dissolution breccias,
774 sedimentary structures representing upper intertidal to supratidal conditions,
775 and well-developed karst surfaces. A few cycles (best shown in C-5) preserve
776 additional features, such as bedded enterolithic anhydrite, which is
777 characteristic of (but not unique to) sabkha environments (Warren 1991, p.
778 175). The succession in the Eilean Dubh Formation studied here provides one
779 of the most complete examples of a Cambrian sabkha. With the presence of
780 former sulfates and marine sediments it would be classed as a coastal sabkha
781 (Handford 1981). The facies, sedimentary structures, and mineralogy of the
782 middle Eilean Dubh Formation compare well with other coastal sabkhas of the
783 Trucial coast (Butler 1969; Curtis et al. 1963; Kinsman 1966, 1969) and of
784 Umm Said, Quatar (Shinn 1973).

785 *Sequence Stratigraphy of the Sauk II to Sauk III Interval in Scotland*

786 The standard sequence stratigraphic model assumes that falling sea
787 level from highstand to lowstand does not leave much record of shallow-
788 marine sediments. To produce the standard model requires an asymmetrical
789 sea-level cycle with a rapid fall (Schlager 2005). This is now known to not be

790 the case, and in many instances there has been significant sediment
791 accumulation during falling sea level, resulting in a falling-stage systems tract
792 (FSST) (Hunt and Tucker 1992; Nummedal et al. 1995; Naish and Kamp
793 1997; Plint and Nummedal 2000; Belopolsky and Droxler 2004). Sandstone
794 FSSTs have also been recorded, beneath the Sauk II–III boundary in
795 Wisconsin and Minnesota (Runkel et al. 2007) and in Arizona (Łabaj and Pratt
796 2016).

797 In the Eilean Dubh Formation, the lower part of the measured section
798 comprises a highstand systems tract (HST), which consists of shallowing-
799 upward cycles and parasequences that record shallow subtidal to lower
800 supratidal facies. There are no karst surfaces, and cycles become
801 increasingly thin up section, but flooding and superposition of deeper water
802 facies always mark the bases. However, at the top of cycle C-4 there is a thin
803 supratidal-flat succession and a sharp erosional cycle boundary that is
804 overlain by sabkha facies (C-5). This major seaward shift in facies belts can
805 be considered to represent offlap and constitutes a regressive surface of
806 marine erosion (RSME). The overlying succession of 10 cycles (C-5 to C-14)
807 generally thin up section and display increasingly prominent karst surfaces at
808 their tops and an increase in abundance of siliciclastic sand. Together the
809 cycles represent falling base level and are an example of a well-preserved
810 FSST. Thinner cycles and increasingly pronounced karst surfaces may
811 represent downstepping (offlapping). In tropical carbonate systems such as
812 this, the downstepping may be due to stillstand or short oscillations of sea
813 level, resulting from carbonates building up to flat topsets (Schlager and
814 Warrlich 2009). Plint and Nummedal (2000) remarked that superimposed

higher-order cycles would result in a number of smaller FSSTs, each with a RSME that recorded forestepping of facies. Only one example in the succession displays forestepping at the cycle boundary, and a karst surface at the top of C-10 is overlain by upper supratidal sabkha facies at the base of C-11.

The sequence boundary at the top of the FSST is taken at the most deeply weathered and most pronounced karst surface, at the top of C-14, and corresponds to the Sauk III–III sequence boundary. Overlying the sequence boundary the succeeding transgressive systems tracts (TST) comprises two very thin intraclast dolorudstones with abundant quartz sand. Above these two cycles (C-15 and C-16), cycles become thicker (c. 1–2 m) and are dominated by subtidal to upper intertidal facies with thick stromatolite biostromes overlain by ripple- and planar-laminated dolostones. Evaporite pseudomorphs are noticeably absent and karst surfaces are less abundant, with only one horizon of karst recorded at the top of C-19.

The FSST in the Scottish section records thinning of the meter-scale upward-shallowing cycles and an increase in the intensity of karst surfaces. This records facies, separated by hiatuses, indicative of deposition under forced regression (Posamentier et al. 1992). Although there are now many documented examples of preservation of FSSTs, they are often not preserved, either due to the rate of sea-level fall being too rapid, the slope being too steep to sustain carbonate production, or accommodation space not being sufficient to allow their preservation. The FSST lies above highstand-systems-tract deposits, and incision must have been minimal to preserve it. Any ravinement on the exposed shelf may have been localized and carried

much of the siliciclastic sediment as bypass (with thin veneers remaining on the platform).

Factors Leading to Preservation of a FSST on the Craton Margin

The preservation of sediment during forced regression should be dependent on the rate of eustatic fall being less than the subsidence rates so that minimal exposure and chemical erosion takes place and accommodation space for further sedimentation is available. Modeling of Laurentian passive-margin subsidence rates indicates the change from high and rapidly decreasing subsidence (95 to 35 m/My) during the Middle Cambrian, to much lower and slowly decreasing subsidence (35 to < 10 m/My) for the Late Cambrian and Early Ordovician (Bond et al. 1989). In the Upper Mississippi Valley where a FSST was documented below the Sauk II–III boundary by Runkel et al. (2007), the epeiric ramp subsided at a rate of < 10 m/My during the Middle Cambrian to Early Ordovician (Sloss 1988), about one-fifth to one-tenth the rate as cratonic margins such as the Appalachian and Cordilleran margins of North America (Hintze and Palmer 1976; Sloss 1988; Miller et al. 2003).

The decline in subsidence rates marks a decline in the thermal subsidence due to increased lithospheric rigidity caused by crustal cooling and thickening (Bond at al. 1988, 1989). The rigidity of the lithosphere can influence the deposition by altering the accommodation space (Reynolds et al. 1991). Scotland had subsidence rates of c. 11 m/My during deposition of the passive-margin carbonates of the Middle to Late Cambrian (Smith and Rasmussen 2008). The relatively low rates in northwest Scotland imply increased rigidity or a very cratonward position. Low flexural rigidity results in

vertical accommodation space and favors the formation of Type 2 sequence boundaries when the rate of sea-level fall is lower than subsidence (Van Wagoner et al. 1988). In contrast, when the rate of fall exceeds the rate of subsidence a Type 1 sequence boundary is more typical (Van Wagoner et al. 1988), and this is expected if the lithosphere is more rigid and accommodation space is broadly distributed across a wider shelf (Reynolds et al. 1991).

Although the karst surface (top C-14) at the sequence boundary is typical of a Type 1 sequence boundary, the preservation of the FSST below suggests that the rate of sea-level fall must have been close to the rate of subsidence, but the karst at many cycle tops leading up to the sequence boundary suggests that sea-level fall surpassed subsidence at times because of the superimposed higher-order cycles on the longer-term trend of Sauk-related shallowing.

Typically a Type 1 sequence boundary is represented by “subaerial exposure and concurrent subaerial erosion, associated with stream rejuvenation, a basinward shift in facies, a downward shift in coastal onlap, and onlap of overlying strata” (Van Wagoner et al. 1987, p. 11). However, in platform carbonates there is evidence that the boundary is sometimes manifested as a sequence-boundary zone rather than a single surface (Osleger and Montañez 1996). The short duration of sea-level fall and then rise as postulated by Saltzman et al. (2004) could be an influencing factor in the preservation of this rare example, since further subaerial exposure and a larger fall in sea-level may eventually have removed all trace of the sabkha.

CONCLUSIONS

889 The Cambrian carbonates of northwest Scotland represent a now isolated but
890 important piece of the history of Laurentia. The middle Eilean Dubh Formation
891 records facies that include intraclast dolorudstones, microbial dolostones,
892 planar- and ripple-laminated dolostones, and siliciclastic siltstones and
893 sandstones. Facies display sedimentary structures common to peritidal
894 sedimentation: mudcracks, ripples, tepees, and planar stromatolites. The
895 facies are arranged into upward-coarsening cycles that become increasingly
896 thin through an interval c. 5.5 m thick (containing 10 cycles) in which
897 siliciclastic sediment caps cycles and karst surfaces become more
898 pronounced. The dolostones comprising the cycles also display a number of
899 evaporite pseudomorphs and probable evaporite dissolution breccias. The
900 presence of peritidal sediments, with pseudomorphs of nodular and bedded
901 anhydrite, vugs from dissolution of sulfate crystals, and halite casts, supports
902 an interpretation of a sabkha depositional environment. The facies are
903 preserved in a FSST beneath the Sauk II–III sequence boundary. The base of
904 the FSST is marked by the first sabkha cycle, which shows a marked
905 progradation of the shoreline and limited erosion of the underlying succession.
906 In common with the Sauk II–III boundary interval at many other localities in
907 Laurentia, the section in the middle Eilean Dubh shows an influx of siliclastic
908 sand. The progradation of a sabkha in Scotland suggests that there was a
909 limited inner detrital belt in comparison with sand sheets and shoreface sands
910 in southern Laurentia that prograded at this time. The Sauk II–III sequence
911 boundary is interpreted to be a Type 1 sequence boundary and to have
912 developed in a location and at a time where tectonic subsidence in Scotland
913 was slow, forcing extensive progradation. The succession of karst surfaces

914 record exposure, during high-order relative sea-level fluctuations, which were
915 imposed on the lower-order, end Sauk II sea-level fall. The rate of sea-level
916 fall must have been close to the subsidence rate and/or the duration of sea-
917 level fall was short and subsequent flooding was rapid to preserve the FSST
918 and the sabkha cycles seen here.

919 Although many cases of evaporite pseudomorphs are recorded from
920 the Cambrian, there are relatively few convincing documented sabkhas, and
921 the middle Eilean Dubh Formation of NW Scotland represents a good ancient
922 analogue.

923 **ACKNOWLEDGMENTS**

924 The authors wish to thank Carl Stevenson and Paul Anderson for their
925 assistance and discussions in the field. The paper was greatly improved by
926 the comments of the reviewers William Morgan, John Luczaj, and Gerome
927 Bellian, associate editor Daniel Lehrmann, and editor Leslie Melim. This work
928 in part results from a PhD conducted by Robert Raine at the University of
929 Birmingham, funded by the School of Geography, Earth and Environmental
930 Sciences and a British Geological Survey BUFI grant (E2152S60).

931 **REFERENCES**

932 AHLBERG, P., AXHEIMER, N., BABCOCK, L. E., ERIKSSON, M. E., SCHMITZ, B., AND
933 TERFELT, F., 2009, Cambrian high-resolution biostratigraphy and carbon
934 isotope chemostratigraphy in Scania, Sweden: first record of the SPICE
935 and DICE excursions in Scandinavia: Lethaia, v. 42, p. 2–16.
936 AITKEN, J.D., 1967, Classification and environmental significance of cryptalgal
937 limestones and dolomites, with illustrations from the Cambrian and

Ordovician of southwestern Alberta: Journal of Sedimentary Petrology, v. 37, p. 1163–1178.

AL-FARRAJ, A., 2005, An evolutionary model for sabkha development on the north coast of the UAE: Journal of Arid Environments, v. 63, p. 740–755.

ALSHARHAN, A.S., AND KENDALL, C.G.ST.C., 1994, Depositional setting of the Upper Jurassic Hith Anhydrite of the Arabian Gulf an analogue to Holocene evaporites of the United Arab Emirates and Lake Macleod of Western Australia: American Association of Petroleum Geologists, Bulletin, v. 78, p. 1075–1096.

ALSHARHAN, A.S., AND KENDALL, C.G.ST.C., 2003, Holocene coastal carbonates and evaporites of the southern Arabian Gulf and their ancient analogues. Earth-Science Reviews, v. 61, p. 191–243.

ARBEY, F., 1980, Les formes de la silice et l'identification des évaporites dans les formations silicifiées: Bulletin du Centres de recherches Exploration–production Elf-Aquitaine, v. 4, p. 309–365.

ASSERETO, R.L.A., AND KENDALL, C.G.ST.C., 1977, Nature, origin and classification of peritidal tepee structures and related breccias: Sedimentology, v. 24, p. 153–210.

BEALES, F.W., AND OLDERSHAW, A.E., 1969, Evaporite-solution brecciation and Devonian carbonate reservoir porosity in western Canada: American Association of Petroleum Geologists, Bulletin, v. 53, p. 503–512.

BELOPOLSKY, A.V., AND DROXLER, A.W., 2004, Seismic expressions and interpretation of carbonate sequences: the Maldives platform, equatorial

962 Indian Ocean: American Association of Petroleum Geologists, Studies
963 in Geology, v. 49, 46 p.
964 BOND, G.C., KOMINZ, M.A., AND GROTZINGER, J.P., 1988, Cambro-Ordovician
965 eustasy: evidence from geophysical modeling of subsidence in
966 Cordilleran and Appalachian passive margins, *in* Kleinspehn, K.L., and
967 Paola, C., eds., New Perspectives in Basin Analysis: New York,
968 Springer-Verlag, p. 129–160.
969 BOND, G.C., KOMINZ, M.A., STECKLER, M.S., AND GROTZINGER, J.P., 1989, Role
970 of thermal subsidence, flexure, and eustasy in the evolution of early
971 Paleozoic passive-margin carbonate platforms, *in* Crevello, P.D.,
972 Wilson, J.L., and Read, J.F., eds., Controls on Carbonate Platform and
973 Basin Development: SEPM, Special Publication 44, p. 39–61.
974 BREZINSKI, D.K., 2004, Stratigraphy of the Frederick Valley and its relationship
975 to karst development: Maryland Geological Survey, Reports of
976 Investigation 75, 100 p.
977 BREZINSKI, D.K., TAYLOR, J.F., AND REPETSKI, J.E., 2012, Sequential
978 development of platform to off-platform facies of the Great American
979 Carbonate Bank in the central Appalachians, *in* Derby, J.R., Fritz, R.D.,
980 Longacre, S.A., Morgan, W.A., and Sternbach, C.A., eds., The Great
981 American Carbonate Bank: The Geology and Economic Resources of
982 the Cambrian–Ordovician Sauk Megasequence of Laurentia: American
983 Association of Petroleum Geologists, Memoir 98, p. 383–420.
984 BUTLER, G.P., 1969, Modern evaporite deposition and geochemistry of
985 coexisting brines, the sabkha, Trucial Coast, Arabian Gulf: Journal of
986 Sedimentary Petrology, v. 39, p. 70–89.

987 BUTLER, G.P., HARRIS, P.M., AND KENDALL, C.G.ST.C., 1982, Recent
988 evaporites from Abu Dhabi coastal flats, *in* Handford, C.R., Robert G.L.,
989 and Graham, R.D., eds., Depositional and Diagenetic Spectra of
990 Evaporites (core workshop no. 3.): Tulsa, Oklahoma, SEPM,. p. 33–64.
991 CAWOOD, P.A., MCCAUSLAND, P.J.A., AND DUNNING, G.R., 2001, Opening
992 Iapetus: Constraints from the Laurentian margin in Newfoundland:
993 Geological Society of America, Bulletin, v. 113, p. 443–453.
994 CHOW, N., AND JAMES, N.P., 1987, Cambrian grand cycles; a northern
995 Appalachian perspective: Geological Society of America, Bulletin, v. 98,
996 p. 418–429.
997 CHOW, N., AND JAMES, N.P., 1992, Synsedimentary diagenesis of Cambrian
998 peritidal carbonates: evidence from hardgrounds and surface paleokarst
999 in the Port au Port Group, western Newfoundland: Bulletin of Canadian
1000 Petroleum Geology, v. 40, p. 115–127.
1001 CHOWNS, T.M., AND ELKINS, J.E., 1974, The origin of quartz geodes and
1002 cauliflower cherts through the silicification of anhydrite nodules: Journal
1003 of Sedimentary Petrology, v. 44, p. 885–903.
1004 CLOYD, K.C, DEMICCO, R.V., AND SPENSER, R.J., 1990, Tidal channel, levee,
1005 and crevasse-splay deposits from a Cambrian tidal channel system: a
1006 new mechanism to produce shallowing-upward sequences: Journal of
1007 Sedimentary Petrology, v. 60, p. 73–83.
1008 COCKS, L.R.M., AND TORSVIK, T.H., 2006, European geography in a global
1009 context from the Vendian to the end of the Palaeozoic, *in* Gee, D.G.,
1010 and Stephenson, R.A., eds., European Lithosphere Dynamics:
1011 Geological Society of London, Memoir 32, p. 83–95.

1012 CODY, R.D., 1976, Growth and early diagenetic changes in artificial gypsum
1013 crystals grown within bentonite muds and gels: Geological Society of
1014 America, Bulletin, v. 87, p. 1163–1168.
1015 COWAN, C.A., AND JAMES, N.P., 1993, The interactions of sea-level change,
1016 terrigenous sediment influx and carbonate productivity as controls of
1017 Upper Cambrian Grand Cycles of western Newfoundland, Canada:
1018 Geological Society of America, Bulletin, v. 105, p. 1576–1590.
1019 COWIE, J.W., 1974, The Cambrian of Spitsbergen and Scotland, *in* Holland,
1020 C.H., ed., Cambrian of the British Isles, Norden and Spitsbergen. Lower
1021 Palaeozoic Rocks of the World, 2: London, John Wiley and Sons, p.
1022 123–155.
1023 CROWLEY, T.J., AND BERNER, R.A., 2001, CO_2 and climate change: Science, v.
1024 292, p. 870–872.
1025 CURTIS, R., EVANS, G., KINSMAN, D.J.J., AND SHEARMAN, D.R., 1963,
1026 Association of dolomite and anhydrite in the recent sediments of the
1027 Persian Gulf: Nature, v. 197, p. 679–680.
1028 DALRYMPLE, R.W., NARBONNE, G.M., AND SMITH, L., 1985, Eolian action and
1029 the distribution of Cambrian shales in North America: Geology, v. 13, p.
1030 607–610.
1031 DAVIES, G.R., 1970, Algal-laminated sediments, Gladstone Embayment,
1032 Shark Bay, Western Australia, *in* Logan, B.W., Davies, G.R., Read, J.F.,
1033 and Cebulski, D.E., eds., Carbonate Sedimentation and Environments,
1034 Shark Bay, Western Australia: American Association of Petroleum
1035 Geologists, Memoir 13, p. 169–205.

1036 DERBY, J.R., RAINE, R.J., SMITH, M.P., AND RUNKEL, A.C., 2012,
1037 Paleogeography of the great American carbonate bank of Laurentia in
1038 the earliest Ordovician (early Tremadocian): The Stonehenge
1039 transgression, *in* Derby, J.R., Fritz, R.D., Longacre, S.A., Morgan, W.A.,
1040 and Sternbach, C.A., eds., The Great American Carbonate Bank: the
1041 Geology and Economic Resources of the Cambrian–Ordovician Sauk
1042 Megasequence of Laurentia: American Association of Petroleum
1043 Geologists, Memoir 98, p. 5–13.
1044 DOTT, R.H., JR., BYERS, C.W., FIELDSER, G.W., STENZEL, S.R., AND WINFREE,
1045 K.E., 1986, Aeolian to marine transition in Cambro-Ordovician cratonic
1046 sheet sandstones of the northern Mississippi valley, U.S.A:
1047 Sedimentology, v. 33, p. 345–367.
1048 EVAMY, B.D., 1973, The precipitation of aragonite and its alteration to calcite
1049 on the Trucial Coast of the Persian Gulf, *in* Purser, B.H., ed., The
1050 Persian Gulf: Berlin, Springer-Verlag, p. 329–342.
1051 EVANS, G., SCHMIDT, V., BUSH, P., AND NELSON, H., 1969, Stratigraphy and
1052 Geologic History of the Sabkha, Abu Dhabi, Persian Gulf:
1053 Sedimentology, v. 12, p. 145–159.
1054 FISCHER, A.G., AND SARNTHEIN, M., 1988, Airborne silts and dune-derived
1055 sands in the Permian of the Delaware basin: Journal of Sedimentary
1056 Petrology, v. 58, p. 637–643.
1057 FOLK, R.L., AND PITTMAN, J.S., 1971, Length-slow chalcedony: a new
1058 testament for vanished evaporites: Journal of Sedimentary Petrology, v.
1059 41, p. 1045–1048.

FORKNER, R.M., 2010, An integrated system for macro-scale anhydrite classification: Geological Quarterly, v. 54, p. 423–430.

FRIEDMAN, G.M., AND SHUKLA, V., 1980, Significance of authigenic quartz euhedra after sulfates: example from the Lockport Formation (Middle Silurian) of New York: Journal of Sedimentary Petrology, v. 50, p. 1299–1304.

GEBELEIN, C.D., 1976, Open marine subtidal and intertidal stromatolites (Florida, the Bahamas and Bermuda), *in* Walter, M.R., ed., Stromatolites: Amsterdam, Elsevier Scientific Publishing Company, Developments in Sedimentology 20, p. 381–388.

GINSBURG, R.N., 1971, Landward movement of carbonate mud: new model for regressive cycles in carbonate. American Association of Petroleum Geologists, Bulletin, v. 55, p. 340.

GLUMAC, B., AND WALKER, K.R., 1998, A Late Cambrian positive carbon-isotope excursion in the southern Appalachians: Relation to biostratigraphy, sequence stratigraphy, environments of deposition, and diagenesis: Journal of Sedimentary Research, v. 68, p. 1212–1222.

GLUMAC, B., AND WALKER, K.R., 2000, Carbonate deposition and sequence stratigraphy of the terminal Cambrian grand cycle in the southern Appalachians: Journal of Sedimentary Research, v. 70, p. 952–963.

GOLDHAMMER, R.K., DUNN, P.A., AND HARDIE, L.A., 1990, Depositional cycles, composite sea level changes, cycle stacking patterns, and the hierarchy of stratigraphic forcing: examples from platform carbonates of the Alpine Triassic: Geological Society of America, Bulletin, v. 102, p. 535–562.

GOLDHAMMER, R.K., LEHMANN, P.J., AND DUNN, P.A., 1993, The origin of high-frequency platform carbonate cycles and third-order sequences (Lower Ordovician El Paso Gp., west Texas): constraints from outcrop data and stratigraphic modeling: Journal of Sedimentary Petrology, v. 63, p. 318–359.

GREY, K., 1989, Handbook for the study of stromatolites and associated structures (second draft): Stromatolite Newsletter, v. 14, p. 82–171.

GROTZINGER, J.P., 1986, Cyclicity and paleoenvironmental dynamics of an early Proterozoic carbonate platform, Rocknest Formation, Wopmay Orogen, N.W.T., Canada: Geological Society of America, Bulletin, v. 97, p. 1208–1231.

HANDFORD, C.R., 1981, A process-sedimentary framework for characterizing Recent and ancient sabkhas: Sedimentary Geology, v. 30, p. 255–265.

HANDFORD, R., LOUCKS, R.G., AND DAVIES, G.R., 1982, Depositional and Diagenetic Spectra of Evaporates: SEPM Core Workshop 3, 395 p.

HANDFORD, C.R., KENDALL, A.C., PREZBINDOWSKI, D.R., DUNHAM, J.B., AND LOGAN, B.W., 1983, Salina – margin tepees, pisoliths and aragonite cements, Lake MacCleod, Western Australia: their significance in had interpreting ancient analogs: Geology, v. 12, p. 523–527.

HARDIE, L.A., 1977, Sedimentation on the Modern Carbonate Tidal Flats of Northwest Andros Island, Bahamas: The Johns Hopkins University Studies in Geology No. 22: Baltimore, The Johns Hopkins University Press, 202 p.

HARDIE, L.A., 1986, Tidal flats, *in* Hardie, L.A., and Shinn, E.A., eds., Carbonate Depositional Environments, Modern and Ancient: Colorado School of Mines Quarterly, v. 81, p. 1–74.

HARDIE, L.A., AND GINSBURG, R.N., 1977, Layering: The origin and environmental significance of lamination and thin bedding, *in* Hardie, L.A., ed., Sedimentation on Modern Carbonate Tidal Flats of Northwest Andros Island, Bahamas: John Hopkins University Studies in Geology, v. 22, p. 50–123.

HINTZE, L.F., AND PALMER, A.R., 1976, Upper Cambrian Orr Formation: Its subdivisions and correlatives in western Utah: U.S. Geological Survey Bulletin 1405-G, 25 p.

HOFFMAN, P., 1976, Stromatolite morphogenesis in Shark Bay, Western Australia, *in* Walter, M.R., ed., Stromatolites: Amsterdam, Elsevier, p. 261–271.

HOFMANN, H.J., 1969, Attributes of Stromatolites: Geological Survey of Canada, Paper 69/39, 58 p.

HUNT, D., AND TUCKER, M.E., 1992, Stranded parasequences and the forced regressive wedge systems tract: Deposition during base-level fall: Sedimentary Geology, v. 81, p. 1–9.

HUSELBEE, M.Y., 1998, Late Cambrian to Earliest Ordovician (Ibexian) Conodont Evolution and Biogeography of Greenland and Northwest Scotland: University of Birmingham, unpublished PhD thesis, 296 p.

HUSELBEE, M.Y., AND THOMAS, A.T., 1998, *Olenellus* and conodonts from the Durness Group, NW Scotland, and the correlation of the Durness succession: Scottish Journal of Geology, v. 34, p. 83–88.

JAMES, N.P., AND STEVENS, R.K., 1986, Stratigraphy and correlation of the Cambro-Ordovician Cow Head Group, western Newfoundland. Geological Survey of Canada, Bulletin 366, 143 p.

JAMES, N.P., STEVENS, R.K., BARNES, C.R., AND KNIGHT, I., 1989, Evolution of a lower Paleozoic continental-margin carbonate platform, northern Canadian Appalachians, *in* Crevello, P.D., Wilson, J.L., and Read, J.F., eds., Controls on Carbonate Platform and Basin Development: SEPM, Special Publication 44, p. 123–146.

JANHERT, R.J., AND COLLINS, L.B., 2012, Characteristics, distribution and morphogenesis of subtidal microbial systems in Shark Bay, Australia: Marine Geology, v. 303–306, p. 106–111.

KAYE, C.A., 1959, Shoreline features and Quaternary shoreline changes, Puerto Rico: U.S. Geological Survey, Professional Paper 317-B, p. 49–140.

KENDALL, C.G.ST.C., 1984, Evaporites, *in* Walker, R.G., ed., Facies Models, 2nd Edition: Geoscience Canada, Reprint Series 1, p. 259–296.

KENDALL, C.G.ST.C., AND SKIPWITH, P.A.D'E., 1968, Recent algal mats of a Persian Gulf lagoon: Journal of Sedimentary Petrology, v. 38, p. 1040–1058.

KENDALL, C.G.ST.C., AND SKIPWITH, P.A.D'E., 1969, Holocene shallow water carbonate and evaporite sediments of Khor Al Bazam, Abu Dhabi, Southwest Persian Gulf: American Association of Petroleum Geologists, Bulletin, v. 53, p. 841–869.

KENDALL, C.G.ST.C., AND WARREN, J., 1987, A review of the origin and setting of tepees and their associated fabrics: Sedimentology, v. 34, p. 1007–1027.

KENNARD, J., 1981, The Arrinthrunga Formation, Georgina Basin, central Australia: Bulletin (Australia. Bureau of Mineral Resources, Geology and Geophysics), v. 211, 61 p.

KINSMAN, D.J.J., 1966, Gypsum and anhydrite of recent age, Trucial Coast, Persian Gulf, *in* Rau, J.L., ed., Symposium on Salt, 2nd: North Ohio Geological Society, v. 1, p. 302–326.

KINSMAN, D.J.J., 1969, Modes of formation, sedimentary associations, and diagnostic features of shallow-water supratidal evaporites: American Association of Petroleum Geologists, Bulletin, v. 53, p. 830–840.

KOERSCHNER, W.F., III, AND READ, J.F., 1989, Field and modeling studies of Cambrian carbonate cycles, Virginia Appalachians: Journal of Sedimentary Petrology, v. 59, p. 654–687.

KOUCHINSKY, A., BENGTSON, S., GALLET, Y., KOROVNIKOV, I., PAVLOV, V., RUNNEGAR, B., AND SHIELDS, G., 2008, The SPICE carbon isotope excursion in Siberia: a combined study of the upper Middle Cambrian–lowermost Ordovician Kulyumbe River section, northwestern Siberian Platform: Geological Magazine, v. 145, p. 609–622.

KRINSLEY, D.H., AND DOORNKAMP, J.C., 1973, Atlas of Quartz Surface Textures: Cambridge, UK, Cambridge University Press, 91 p.

ŁABAJ, M.A., AND PRATT, B.R., 2016, Depositional dynamics in a mixed carbonate–siliciclastic system: Middle–Upper Cambrian Abrigo

Formation, southeastern Arizona, U.S.A: Journal of Sedimentary Research, v. 86, p. 11–37.

LAUGHREY, C.D., 1994, Sedimentary evaporites in the Gatesburg Formation of Central Pennsylvania: Pennsylvania Geology, v. 25, p.10–15.

LOCHMAN-BALK, C., 1971, Cambrian of the craton, *in* Holland, E.R., ed., Cambrian of the New World: London, Wiley-Interscience, p. 79–167.

LOGAN, B.W., 1961, Cryptozoon and associate stromatolites from the Recent of Shark Bay, Western Australia: Journal of Geology, v. 69, p. 517–533.

LOGAN, B.W., HOFFMAN, P., AND GEBELEIN, C.D., 1974, Algal mats, cryptalgal fabrics, and structures, Hamelin Pool, Western Australia, *in* Logan, B.W., Read, J.F., Hagan, G.M., Hoffman, P., Brown, R.G., Woods, P.J., and Gebelein, C.D., eds., Evolution and Diagenesis of Quaternary Carbonate Sequences, Shark Bay, Western Australia: American Association of Petroleum Geologists, Memoir 22, p. 140–194.

LOKIER, S., AND STEUBER, T., 2009, Large-scale intertidal polygonal features of the Abu Dhabi coastline: Sedimentology, v. 56, p. 609–621.

LUCIA, F.J., 1961, Dedolomitization in the Tansill (Permian) Formation: Geological Society of America, Bulletin, v. 72, p. 1107–1110.

MACNAUGHTON, R.B., DALRYMPLE, R.W., AND NARBONNE, G.M., 1997, Multiple orders of relative sea-level change in an earliest Cambrian passive-margin succession, Mackenzie Mountains, northwestern Canada: Journal of Sedimentary Research, v. 67, p. 622–637.

MAIKLEM, W.R., BEBOUT, D.G., AND GLAISTER, R.P., 1969, Classification of anhydrite: a practical approach: Bulletin of Canadian Petroleum Geology, v. 17, p. 194–233.

MARKELLO, J.R., AND READ, J.F., 1981, Carbonate ramp-to-deeper shale shelf transitions of an Upper Cambrian intrashelf basin, Nolichucky Formation, Southwest Virginia Appalachians: Sedimentology, v. 28, p. 573–597.

MATTI, J.C., AND MCKEE, E.D., 1976, Stable eustasy, regional subsidence and a carbonate factory: self-regulating model for onlap-offlap cycles in shallow water carbonate sequences: Geological Society of America, Abstracts with Programs, v. 8, p. 1000–1001.

MILLER, J.F., EVANS, K.R., LOCH, J.D., ETHINGTON, R.L., STITT, J.H., HOLMER, L., AND POPOV, L.E., 2003, Stratigraphy of the Sauk III interval (Cambrian–Ordovician) in the Ibex area, western Millard County, Utah and Central Texas: Brigham Young University Geology Studies, v. 47, p. 23–118.

MILLER, K.G., KOMINZ, M.A., BROWNING, J.V., WRIGHT, J.D., MOUNTAIN, G.S., KATZ, M.E., SUGARMAN, P.J., CRAMER, B.S., CHRISTIE-BLICK, N., AND PEKAR, S.F., 2005, The Phanerozoic record of global sea-level change: Science, v. 310, p. 1293–1298.

MILLIKEN, K., 1979, The silicified evaporite syndrome—two aspects of silicification history of former evaporite nodules from southern Kentucky and northern Tennessee: Journal of Sedimentary Petrology, v. 49, p. 245–256.

MONTAÑEZ, I.P., AND OSLEGER, D.A., 1993, Parasequence stacking patterns, third-order accommodation events, and sequence stratigraphy of Middle to Upper Cambrian platform carbonates, Bonanza King Formation, southern Great Basin, *in* Loucks, R.G., and Sarg, J.F., eds., Carbonate

Sequence Stratigraphy: Recent Developments and Applications: American Association of Petroleum Geologists, Memoir 57, p. 305–326.

MONTAÑEZ, I.P., AND OSLEGER, D.A., 1996, Contrasting sequence boundary zones developed within cyclic carbonates of the Bonanza King Formation, Middle to Late Cambrian, southern Great Basin, *in* Witzke, B.J., Ludvigson, G.A., and Day, J., eds., Paleozoic Sequence Stratigraphy: Views from the North American Craton: Geological Society of America, Special Paper 306, p. 7–21.

MORGAN, W.A., 2012, Sequence stratigraphy of the great American carbonate bank, *in* Derby, J.R., Fritz, R.D., Longacre, S.A., Morgan, W.A., and Sternbach, C.A., eds., The Great American Carbonate Bank: the Geology and Economic Resources of the Cambrian–Ordovician Sauk Megasequence of Laurentia: American Association of Petroleum Geologists, Memoir 98, p. 37–82.

MORROW, D.W., 1982, Descriptive field classification of sedimentary and diagenetic breccia fabrics in carbonate rocks: Bulletin of Canadian Petroleum Geology, v. 30, p. 227–229.

MOSSOP, G.D., 1979, The evaporites of the Ordovician Baumann Fiord Formation, Ellesmere Island, Arctic Canada: Geological Survey of Canada, Bulletin 298, 52 p.

MOUNT, J., 1985, Mixed siliciclastic and carbonate sediments: a proposed first-order textural and compositional classification: Sedimentology, v. 32, p. 435–442.

MOUNT, J.F., AND KIDDER, D., 1993, Combined flow origin of edgewise intraclast conglomerates: Sellick Hill Formation (Lower Cambrian), South Australia: Sedimentology, v. 40, p. 315–329.

NAISH, T., AND KAMP, P.J.J., 1997, Sequence stratigraphy of sixth-order (41 k.y.) Pliocene–Pleistocene cyclothems, Wanganui basin, New Zealand: A case for the regressive systems tract: Geological Society of America, Bulletin, v. 109, p. 978–999.

NUMMEDAL, D., GUPTA, S., PLINT, A.G., AND COLE, R.D., 1995, The falling stage systems tract: definition, character and expression in several examples from the Cretaceous from the U.S. Western Interior, *in* Hunt, D., Gawthorpe, R.L., and Dogherty, M., eds., Sedimentary Responses to Forced Regressions, Abstract Volume: London, Geological Society, p. 45–48.

OSLEGER, D., 1991, Subtidal carbonate cycles: Implications for allocyclic vs. autocyclic controls: Geology, v. 19, p. 917–920.

OSLEGER, D.A., AND MONTAÑEZ, I.P., 1996, Cross-platform architecture of a sequence boundary in mixed siliciclastic–carbonate lithofacies, Middle Cambrian, southern Great Basin, USA: Sedimentology, v. 43, p. 197–217.

OSLEGER, D., AND READ, J.F., 1991, Relation of eustasy to stacking patterns of meter-scale carbonate cycles, Late Cambrian, USA: Journal of Sedimentary Petrology, v. 61, p. 1225–1252.

OSLEGER, D., AND READ, J.F., 1993, Comparative analysis of methods used to define eustatic variations in outcrop; Late Cambrian: American Journal of Science, v. 293, p. 157–216.

PALMER, A.R., 1960, Some aspects of the early Upper Cambrian stratigraphy of White Pine County, Nevada, and Vicinity, in Geology of east central Nevada: Intermountain Association of Petroleum Geologists, 11th Annual Field Conference, Guidebook, p. 53–58.

PALMER, A.R., 1971a, The Cambrian of the Appalachian and eastern New England regions, eastern United States, *in* Holland, C.H., ed., Cambrian of the New World: London, Wiley Interscience, p. 169–217.

PALMER, A.R., 1971b, The Cambrian of the Great Basin and adjacent areas, western United States, *in* Holland, C.H., ed., Cambrian of the New World: London, Wiley Interscience, p. 1–79.

PALMER, A.R., 1981, Subdivision of the Sauk sequence: U.S. Geological Survey, Open-File Report 81-743, p. 160–162.

PATTERSON, R.J., AND KINSMAN, D.J.J., 1981, Hydrologic framework of a sabkha along Arabian Gulf: American Association of Petroleum Geologists, Bulletin, v. 65, p. 1457–1475.

PATTERSON, R.J., AND KINSMAN, D.J.J., 1982, Formation of diagenetic dolomite in coastal sabkha along Arabian (Persian) Gulf: American Association of Petroleum Geologists, Bulletin, v. 66, p. 28–43.

PLINT, A.G., AND NUMMEDAL, D., 2000, The falling stage systems tract: Recognition and importance in sequence stratigraphic analysis, *in* Hunt, G., and Gawthorpe, R.L., eds., Sedimentary Responses to Forced Regressions: Geological Society of London, Special Publication 172, p. 1–17.

POSAMENTIER, H.W., ALLEN, G.P., JAMES, D.P., AND TESSON, M., 1992, Forced regressions in a sequence stratigraphic framework: Concepts,

examples, and exploration significance: American Association of Petroleum Geologists Bulletin, v. 76, p. 1687–1709.

PRATT, B.R., AND JAMES, N.P., 1986, The St. George Group (Lower Ordovician) of western Newfoundland: tidal flat island model for carbonate sedimentation in shallow epeiric seas: Sedimentology, v. 33, p. 313–343.

PURSER, B.H., ed., 1973, The Persian Gulf: Berlin, Springer-Verlag, 471 p.

RADKE, B.M., AND MATHIS, R.L., 1980, On the formation and occurrence of saddle dolomite: Journal of Sedimentary Petrology, v. 50, p. 1149–1168.

RAINE, R.J., AND SMITH, M.P., 2012, Sequence stratigraphy of the Scottish Laurentian margin and recognition of the Sauk Megasequence, *in* Derby, J.R., Fritz, R.D., Longacre, S.A., Morgan, W.A., and Sternbach, C.A., eds., The Great American Carbonate Bank: the Geology and Economic Resources of the Cambrian–Ordovician Sauk Megasequence of Laurentia: American Association of Petroleum Geologists, Memoir 98, p. 575–596.

READ, J.F., 1989, Controls on evolution of Cambrian–Ordovician passive margin, U.S. Appalachians, *in* Crevello, P.D., Wilson, J.L., and Read, J.F., eds., Controls on Carbonate Platform and Basin Development: SEPM, Special Publication 44, p. 147–165.

READ, J.F., AND GROVER, G.A., 1977, Scalloped and planar erosion surfaces, Middle Ordovician limestones, Virginia: analogues of Holocene exposed karst or tidal rock platforms: Journal of Sedimentary Petrology, v. 47, p. 956–972.

1327 REYNOLDS, D.J., STECKLER, M.S., AND COAKLEY, B.J., 1991, The role of
1328 sediment load in sequence stratigraphy: The influence of flexural
1329 isostasy and compaction: Journal of Geophysical Research, v. 96, p.
1330 6931–6949.
1331 RUNKEL, A.C., MCKAY, R.M., AND PALMER, A.R., 1998, Origin of a classic
1332 cratonic sheet sandstone: Stratigraphy across the Sauk II–Sauk III
1333 boundary in the Upper Mississippi Valley: Geological Society of
1334 America, Bulletin, v. 110, p. 188–210.
1335 RUNKEL, A.C., MILLER, J.F., MCKAY, R.M., PALMER, A.R., AND TAYLOR, J.F.,
1336 2007, High-resolution sequence stratigraphy of lower Paleozoic sheet
1337 sandstones in central North America: The role of special conditions of
1338 cratonic interiors in development of strata architecture: Geological
1339 Society of America, Bulletin, v. 119, p. 860–881.
1340 SALTZMAN, M.R., RUNNEGAR, B., AND LOHMANN, K.C., 1998, Carbon isotope
1341 stratigraphy of Upper Cambrian (Steptoean Stage) sequences of the
1342 eastern Great Basin; record of a global oceanographic event:
1343 Geological Society of America, Bulletin, v. 110, p. 285–297.
1344 SALTZMAN, M.R., RIPPERDAN, R.L., BRASIER, M.D., LOHMANN, K.C., ROBINSON,
1345 R.A., CHANG, W.T., PENG, S., ERGALIEV, E.K., AND RUNNEGAR, B., 2000, A
1346 global carbon isotope excursion (SPICE) during the Late Cambrian:
1347 relation to trilobite extinctions, organic-matter burial and sea level:
1348 Palaeogeography, Palaeoclimatology, Palaeoecology, v. 162, p. 211–
1349 223.
1350 SALTZMAN, M.R., COWAN, C.A., RUNKEL, A.C., RUNNEGAR, B., STEWART, M.C.,
1351 AND PALMER, A.R., 2004, The Late Cambrian Spice ($\delta^{13}C$) event and the

1352 Sauk II–Sauk III regression: New evidence from Laurentian basins in
1353 Utah, Iowa, and Newfoundland: Journal of Sedimentary Research, v.
1354 74, p. 366–377.
1355 SCHLAGER, W., 2004, Fractal nature of stratigraphic sequences: Geology, v.
1356 32, p. 185–188.
1357 SCHLAGER, W., 2005, Carbonate Sedimentology and Sequence Stratigraphy:
1358 SEPM, Concepts in Sedimentology and Paleontology No. 8, 200 p.
1359 SCHLAGER, W., AND WARRLICH, G., 2009, Record of sea-level fall in tropical
1360 carbonates: Basin Research, v. 21, p. 209–224.
1361 SCHNEIDER, J., 1976, Biological and inorganic factors in the destruction of
1362 limestone coasts: Contributions to Sedimentology 6, 1–112.
1363 SCOTESE, C.R., 2009, Late Proterozoic plate tectonics and palaeogeography:
1364 a tale of two supercontinents, Rodinia and Pannotia, *in* Craig, J.,
1365 Thurow, J., Thusu, B., Witham, A., and Abutarruma, Y., eds., Global
1366 Neoproterozoic Petroleum Systems: The Emerging Potential in North
1367 Africa: Geological Society of London, Special Publication 326, p. 67–83.
1368 SHINN, E.A., 1968, Practical significance of birdseye structures in carbonate
1369 rocks: Journal of Sedimentary Petrology, v. 38, p. 215–223.
1370 SHINN, E.A., 1973, Sedimentary accretion along the leeward, S.E. coast of
1371 Qatar peninsula, Persian Gulf, *in* Purser, B.H., ed., The Persian Gulf:
1372 Berlin, Springer, p. 199–209.
1373 SHINN, E.A., 1983, Tidal flat environment, *in* Scholle, P.A., Bebout, D.G., and
1374 Moore, C.H., eds., Carbonate Depositional Environments: American
1375 Association of Petroleum Geologists, Memoir 33, p. 171–210.

SHINN, E.A., 1986, Modern carbonate tidal flats: their diagnostic features, *in* Hardie, L.A., and Shinn, E.A., eds., Carbonate Deposltional Environments. Modern and Ancient. Part 3: Tidal Flats: Colorado School of Mines Quarterly, v. 81/1, p. 17–36.

SHINN, E.A., LLOYD, R.M., AND GINSBURG, R.N., 1969, Anatomy of a modern carbonate tidal-flat, Andros Island, Bahamas: Journal of Sedimentary Petrology, v. 39, p. 1202–1228.

SIAL, A.N., PERALTA, S., FERREIRA, V.P., TOSELLI, A.J., ACEÑOLAZA, F.G., PARADA, M.A., GAUCHER, C., ALONSO, R.N., AND PIMENTEL, M.M., 2008, Cambrian carbonate sequences of the Argentine Precordillera and the Steptoean C-Isotope positive excursion (SPICE): Gondwana Research, v. 13, p 437–452.

SIAL, A.N., PERALTA, S., GAUCHER, C., TOSELLI, A.J., FERREIRA, V.P., FREI, R., PARADA, M.A., PIMENTEL, M.M., AND PEREIRA, N.S., 2013, High-resolution stable isotope stratigraphy of the Upper Cambrian and Ordovician in the Argentine Precordillera: Carbon isotope excursions and correlations: Gondwana Research, v. 24, p. 330–348.

SIEDLECKA, A., 1972, Length-slow chalcedony and relicts of sulfates—evidence of evaporitic environments in the Upper Carboniferous and Permian beds of Bear Island, Svalbard: Journal of Sedimentary Petrology, v. 42, p. 812–816.

SIEDLECKA, A., 1976, Silicified Precambrian evaporite nodules from northern Norway: a preliminary report: Sedimentary Geology, v. 16, p. 161–175.

SLOSS, L.L., 1963, Sequences in the cratonic interior of North America: Geological Society of America, Bulletin, v. 74, p. 93–114.

SLOSS, L.L., 1988, Tectonic evolution of the craton in Phanerozoic time, *in* Sloss, L.L., ed., Sedimentary Cover–North American Craton, United States: Boulder, Colorado, Geological Society of America, Geology of North America, v. D-2, p. 25–51.

SMITH, M.P., AND RASMUSSEN, J.A., 2008, Cambrian–Silurian development of the Laurentian margin of the Iapetus Ocean in Greenland and related areas, *in* Higgins, A.K., Gilotti, J.A., and Smith, M.P., eds., The Greenland Caledonides: Evolution of the Northeast Margin of Laurentia: Geological Society of America, Memoir 202, p. 137–167.

SWEETING, M.M., 1972, Karst Landforms: New York, Columbia University Press, 362 p.

SWETT, K., 1981, Cambro-Ordovician strata in Ny Friesland, Spitsbergen and their palaeotectonic significance: Geological Magazine, v. 118, p. 225–250.

SWETT, K., AND SMIT, D.E., 1972a, Paleogeography and depositional environments of the Cambro-Ordovician shallow-marine facies of the North Atlantic: Geological Society of America, Bulletin, v. 83, p. 3223–3248.

SWETT, K., AND SMIT, D.E., 1972b, Cambro-Ordovician shelf sedimentation of western Newfoundland, northwest Scotland and central East Greenland: 24th Session, International Geological Congress, v. 6, p. 33–41.

TAYLOR, J.F., BREZINSKI, D.K., REPETSKI, J.E., AND WELSH, N.M., 2009, The Adamstown submergence event: Faunal and sedimentological record of a Late Cambrian transgression in the Appalachian Region, *in* Laurie,

J.R., ed., Cambro-Ordovician Studies IV: Association of Australasian Palaeontologists, Memoirs 34, p. 147–156.

TORSVIK, T.H., SMETHURST, M.A., MEERT, J.G., VAN DER VOO, R., MCKERROW, W.S., BRASIER, M.D., STURT, B.A., AND WALDERHAUG, H.J., 1996, Continental break-up and collision in the Neoproterozoic and Palaeozoic: A tale of Baltica and Laurentia: Earth-Science Reviews, v. 40, p. 229–258.

TUCKER, M.E., 1976a, Quartz replaced anhydrite nodules ('Bristol Diamonds') from the Triassic of the Bristol District: Geological Magazine, v. 113, p. 569–574.

TUCKER, M.E., 1976b, Replaced evaporites from the late Precambrian of Finnmark, Arctic Norway: Sedimentary Geology, v. 16, p. 193–204.

VAN WAGONER, J.C., MITCHUM, R.M., POSAMENTIER, H.W., AND VAIL, P.R., 1987, Seismic stratigraphy interpretation using sequence stratigraphy. Part 2: key definitions of sequence stratigraphy, *in* Balley, A.W., ed., Atlas of Seismic Stratigraphy: American Association of Petroleum Geologists, Studies in Geology 27-1, p. 11–13.

VAN WAGONER, J.C., POSAMENTIER, H.W., MITCHUM, R.M., VAIL, P.R., SARG, J.F., LOUTIT, T.S., AND HARDENBOL, J., 1988, An overview of the fundamentals of sequence stratigraphy and key definitions, *in* Wilgus, C.K., Hastings, B.S., Kendall, C.G.St.C., Posamentier, H.W., Ross, C.A., and Van Wagoner, J.C., eds., Sea-Level Changes: an Integrated Approach: SEPM, Special Publications 42, p. 39–45.

VAN WAGONER, J.C., MITCHUM, R.M., CAMPION, K.M., AND RAHMANIAN, V.D., 1990, Siliciclastic Sequence Stratigraphy in Well Logs, Cores, and

Outcrops: Concepts for High-Resolution Correlation of Time and Facies: American Association of Petroleum Geologists, Methods in Exploration 7, 55 p.

WARREN, J.K., 1991, Sulfate dominated sea-marginal and platform evaporative settings, *in* Melvin, J.L., ed., Evaporites, Petroleum and Mineral Resources: Amsterdam, Elsevier, Developments in Sedimentology 50, p. 477–533.

WARREN, J.K., 2006, Evaporites; Sediments, Resources and Hydrocarbons: Berlin, Springer, 1036 p.

WARREN, J.K., AND KENDALL, C.G.ST.C., 1985, Comparison of sequences formed in marine sabkha (subaerial) and salina (subaqueous) settings–modern and ancient: American Association of Petroleum Geologists, Bulletin, v. 69, p. 1013–1023.

WATERS, B.B., SPENCER, R.J., AND DEMICCO, R.V., 1989, Three-dimensional architecture of shallowing-upward carbonate cycles: Middle and Upper Cambrian Waterfowl Formation, Canmore, Alberta: Bulletin of Canadian Petroleum Geology, v. 37, p. 198–209.

WEST, I.M., 1964, Evaporite diagenesis in the Lower Purbeck Beds of Dorset: Yorkshire Geological Society, Proceedings, v. 34, p. 315–330.

WESTROP, S.R., 1992, Upper Cambrian (Marjuman–Steptoean) trilobites from the Port au Port Group, Western Newfoundland: Journal of Paleontology, v. 66, p. 228–255.

WILSON, I., 1971, Desert sandflow basins and a model for the development of ergs: Geographical Journal, v. 137, p. 180–199.

1474 WOODS, M.A., WILBY, P.R., LENG, M.J., RUSHTON, A.W.A., AND WILLIAMS, M.,
1475 2011, The Furongian (late Cambrian) Steptoean Positive Carbon
1476 Isotope Excursion (SPICE) in Avalonia: Geological Society of London,
1477 Journal, v. 168, p. 851–862.
1478 WRIGHT, D.T., AND KNIGHT, I., 1995, A revised chronostratigraphy for the lower
1479 Durness Group: Scottish Journal of Geology, v. 31, p. 11–22.
1480 YOUNG, H.R., 1979, Evidence of former evaporites in the Cambro-Ordovician
1481 Durness Group, Northwest Scotland: Sedimentary Geology, v. 22, p.
1482 287–303.

FIGURE CAPTIONS

Fig. 1.—A) Map showing the location of the study area (Balnakeil Bay, Durness) in relation to the Caledonian Moine Thrust zone and the Cambro-Ordovician outcrop (modified after Raine and Smith 2012). B) Detailed location map displaying the geology, local settlements, and named landmarks. The red dot marks the 20 m main section measured here and two supplementary sections, which are situated at the western end of Balnakeil Bay. The Durness Group in this area represents a down-faulted graben and is faulted against mylonites of the Moine Thrust zone.

Fig. 2.—Stratigraphy of the Durness Group and position of the study sections (marked by the red box). The dark blue color represents carbonates dominated by subtidal facies. The light blue colors represent peritidal carbonate facies. Siliciclastic sandstones (yellow) and siltstones (green) make up the underlying Sauk I Ardvreck Group. The sequence boundaries are shown, along with a relative-sea-level curve and the divisions of the Sauk Megasequence (modified after Raine and Smith 2012).

Fig. 3.—Sedimentary log of the study interval (main section) with facies associations and cycles marked. The carbonates are composed entirely of dolomite, but chert intervals, siliciclastic sediment, and prominent karst surfaces are indicated. The interval spans the regressive surface of marine erosion (RSME) and the falling-stage systems tract (FSST), with the

interpreted Sauk II–III sequence boundary (SB) shown. The facies-association codes refer to those described in the paper.

Fig. 4.—Intraclast dolorudstone facies association. A) Intraclasts in a shallow channel cut; cycle 18; hammer is 33 cm long. B) Edgewise mud clasts. There are some gently curved examples suggesting an origin through erosion of mud-cracked tidal flats. The rudstone displays a fan-shaped arrangement of clasts; cycle 22; scale bar is in cm. C) Clast-supported dolorudstone containing two layers of clasts, which become progressively more inclined upwards. The clasts are coarser grained than the matrix and weather proud; cycle 4. D) Dolorudstone with a flat base and slightly mounded top, with a matrix of quartz-sand-rich dolomite. The bed is laterally equivalent to a dolorudstone with larger intraclasts, associated with karst pinnacles in cycle 20; tape measure is 9 cm wide. E) Dolorudstone from below the measured section containing rounded clasts (suggesting moderate reworking) in a quartz arenaceous matrix. The dolorudstone displays a sharp irregular base and directly overlies mud-cracked and rippled, light gray dolostones of lithology similar to that of the clasts; the lens cap is 7 cm in diameter.

Fig. 5.—Microbial dolostone facies association. A) Domal biostromes of digitate, columnar branching stromatolites in cycle 4; scale is in cm. B) Polished block of the stromatolite biostromes in Part A. The margins of the stromatolites are well defined and constringed. They locally display branching and new stromatolites have formed on irregular erosional surfaces (arrowed). C) Domes on the top of a stromatolite bioherm in cycle 6; hammer is 33 cm

long. D) Irregular karst surface (arrow), which is overlain by “encrusting” linked, low-relief, hemispheroidal stromatolite bioherms; pencil is 15 cm long.

Fig. 6.—Ripple-laminated to planar-laminated dolostone facies association and associated structures. A) Ripple-laminated heterolith showing wavy bedding, with low-amplitude current ripples; cycle 10; pencil is 15 cm long. B) Plan view of a bed displaying symmetrical wave ripples (1), which is immediately overlain by a bed containing ripples with a different paleocurrent orientation (2); cycle 22; scale is 7 cm long. C) Ripple lamination observed towards the top of cycle 18 showing scour and drape (white arrows). Quartz silt and sand rests in the scour (black arrow). D) Loose block of parallel-laminated, light gray dolostone with desiccation cracks, which form polygons extending over an area 30 cm in diameter; 7 cm lens cap for scale. E) Ripple cross-lamination traced out by quartz grains in the lower half of the image (black arrows). The upper part shows a scalloped karst surface (white arrow) overlain by intraclast rudstone, the matrix of which contains abundant quartz sand grains; cycle 17. F) Peritidal tepee showing deformation of c. 30 cm thickness of sediment. There is some overthrusting of the crust and some bedding-parallel sheet cracks are present (arrowed); cycle 20.

Fig. 7.—Siliciclastic sandstone and siltstone facies association. A) Irregular bed of gray-purple siltstone, which drapes an irregular surface and thickens in the depressions (1). Overlying the siltstone is a well-sorted, dolomite-cemented sandstone containing “millet-seed” medium to very coarse quartz sand grains (2). The siltstone and sandstone beds represent C-13, and the

underlying and overlying cycles are labelled; scale bar is 5 cm. B) Bed of dark gray siltstone (9 cm thick) at the base of cycle 8; pencil is 15 cm long.

Fig. 8.—Evaporite crystal pseudomorphs. A) Brecciated and deformed, laminated dolostone clasts in a matrix of crystal-vug-rich dolostone. The growth of evaporite (subsequently dissolved) crystals in the sediment may be responsible for the observed deformation; cycle 5. B) A vuggy bed displaying soft sediment deformation associated with the crystal-shaped vugs; cycle 5; pencil is 14 cm long. C) Highly vuggy dolostone caused by dissolution of numerous crystal-shaped vugs; cycle 5. D) Lens-shaped bed containing crystal vugs, which is overlain by contorted bed of dolomite, interpreted to be pseudomorphed anhydrite; cycle 5.

Fig. 9.—A) Tabular and lenticular vugs (former sulfate crystals) in columnar digitate stromatolites, cycle 4. B) Thin-section photomicrograph of finely crystalline nonferroan dolomite containing nonferroan calcite spar (arrows), presumably filling a void following dissolution of a sulfate crystal precursor; plane-polarized light; cycle 5. C) Abundant crystal pseudomorphs, represented by vugs on the weathered surface; cycle 5; scale bar is 1 cm. D) Hand specimen from a vertical surface in cycle 5 (probably a desiccation crack). Along the surface elongate vugs show the shape of the precursor evaporite crystals. Locally evidence of twinning is seen (arrowed); scale is in cm.

1582 Fig. 10.—Evaporite nodule pseudomorphs. A) White knobbly quartz nodules,
1583 which are observed in deformed dolostone. The deformed dolostone shows a
1584 sharp boundary with laminated dolostone containing quartz grains; cycle 5. B)
1585 Dolomite bed with a texture attributable to a contorted anhydrite nodule. The
1586 anhydrite is now replaced by fine-grained dolomite, but the texture is visible
1587 because of residual iron oxyhydroxides; cycle 11. C) Nodule margin
1588 displaying a transition from chalcedony (lutecite) (chal) to megaquartz (qtz)
1589 and minor nonferroan calcite (nfc); crossed-polarized light; cycle 5. D) Dusty
1590 margins of the quartz crystals preserve the “felted lath” texture of the original
1591 precursor anhydrite; plane-polarized light; cycle 5.
1592
1593 Fig. 11.—Pseudomorphs of bedded anhydrite. A) Dolostone bed, which
1594 displays a “lumpy” internally deformed texture. The bed is tightly folded
1595 (arrowed), highlighted by an orange chert layer. The dolostone is interpreted
1596 as a replacement of bedded, enterolithic anhydrite; cycle 5; tape measure is 9
1597 cm wide. B) Plan view of the top of the bed shown in Part A. The chert shows
1598 a circular arrangement, which may indicate planing off of the anhydrite bed
1599 attributed to deflation of the sabkha. C) Beds representing cycle 13 (between
1600 the two white lines) display the “lumpy” texture seen in the bed in cycle 5.
1601 These beds are also interpreted to be replaced bedded anhydrite due to the
1602 similar texture and the lateral red-chert-cemented dolomite (?collapse)
1603 breccias (arrow); the pencil is 15 cm long.
1604
1605 Fig. 12.—Halite casts from cycle 6. A) Bedding plane displaying an irregular
1606 surface with poorly defined halite casts, interpreted to be a halite crust. B)

Dolostone cast of the corner of a halite hopper; specimen is inverted; scale bar is in cm. C) Dolostone cast of the impression of a composite halite hopper; specimen is inverted; scale bar is in cm. D) Small casts of halite crystals (h) associated with mudcracks (m) on an inverted specimen; scale bar is in cm.

Fig. 13.—Breccias interpreted to be formed during the dissolution of evaporites. A) Rubble packbreccia that, laterally, contains evaporite crystal pseudomorphs; cycle 5. B) Mosaic packbreccia composed of dolostone and angular red chert clasts (arrow); cycle 5. C) Crackle to mosaic packbreccia, with a smooth base and irregular upper surface (dashed lines); lens cap is 7 cm in diameter. D) Floatbreccia comprising angular clasts in a hematite-rich chert-replaced matrix. The breccia is laterally equivalent of beds interpreted to be pseudomorphed bedded anhydrite; cycle 13; tape measure is 9 cm in diameter.

Fig. 14.—Karst features. A) Two karst surfaces marking the upper boundaries of cycles 12 and 13. The karst at the top of C-12 is pronounced and comprises pinnacles separated by curved depressions. The depressions are filled by microbial dolostone (arrowed). The pronounced karstic surface is laterally equivalent to a bed of pseudomorphed bedded anhydrite; 55 cm of rule visible. B) Karstic fissure at the boundary between cycles 14 and 15. The hollow is filled by dolostone with abundant quartz sand and local pebbles of dolostone. The red color at the top of the fissure fill is hematite-cemented silty dolostone. C) Rubbly and conglomeratic dolostone, which is laterally

equivalent of a siliciclastic siltstone overlying a karst surface. The conglomerate is interpreted to represent a regolith deposit; cycle 11. D) Mound-shaped pinnacle caused by karstic weathering of a pre-existing stromatolite bioherm. The pinnacle is flanked (boundary arrowed) by conglomerate containing a range of angular pebble- to cobble-grade angular clasts; boundary between cycle 19 and 20; hammer is 33 cm long. E) Vugs and voids filled with pink calcite spar. The voids are developed within a stromatolite bioherm on top of which there is a karst surface; cycle 19.

Fig. 15.—Correlation of the main measured section with two supplementary sections (distances apart are shown) across the sequence-boundary zone (Sauk II–III), showing the facies associations and cycles. Some of the cycles are locally absent, and there is a broad increase in thickness and completeness of the cycles from section A to section B. Distribution of quartz sand is shown (Q). Numbers are not shown on the thinnest cycles. The sections are flattened on the sequence boundary (dashed line).

Figure 1

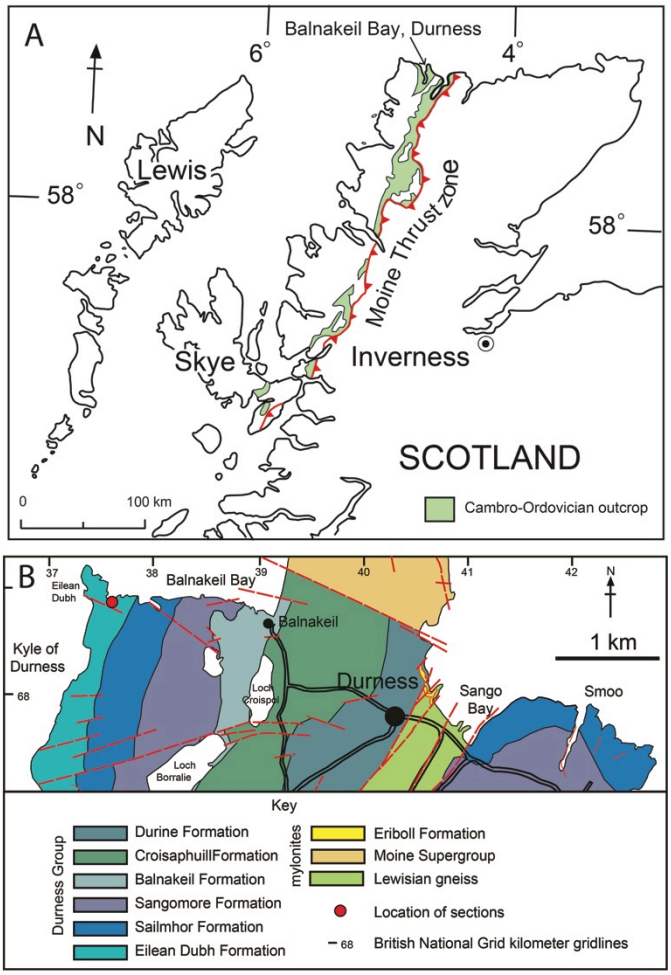

1649

Figure 2

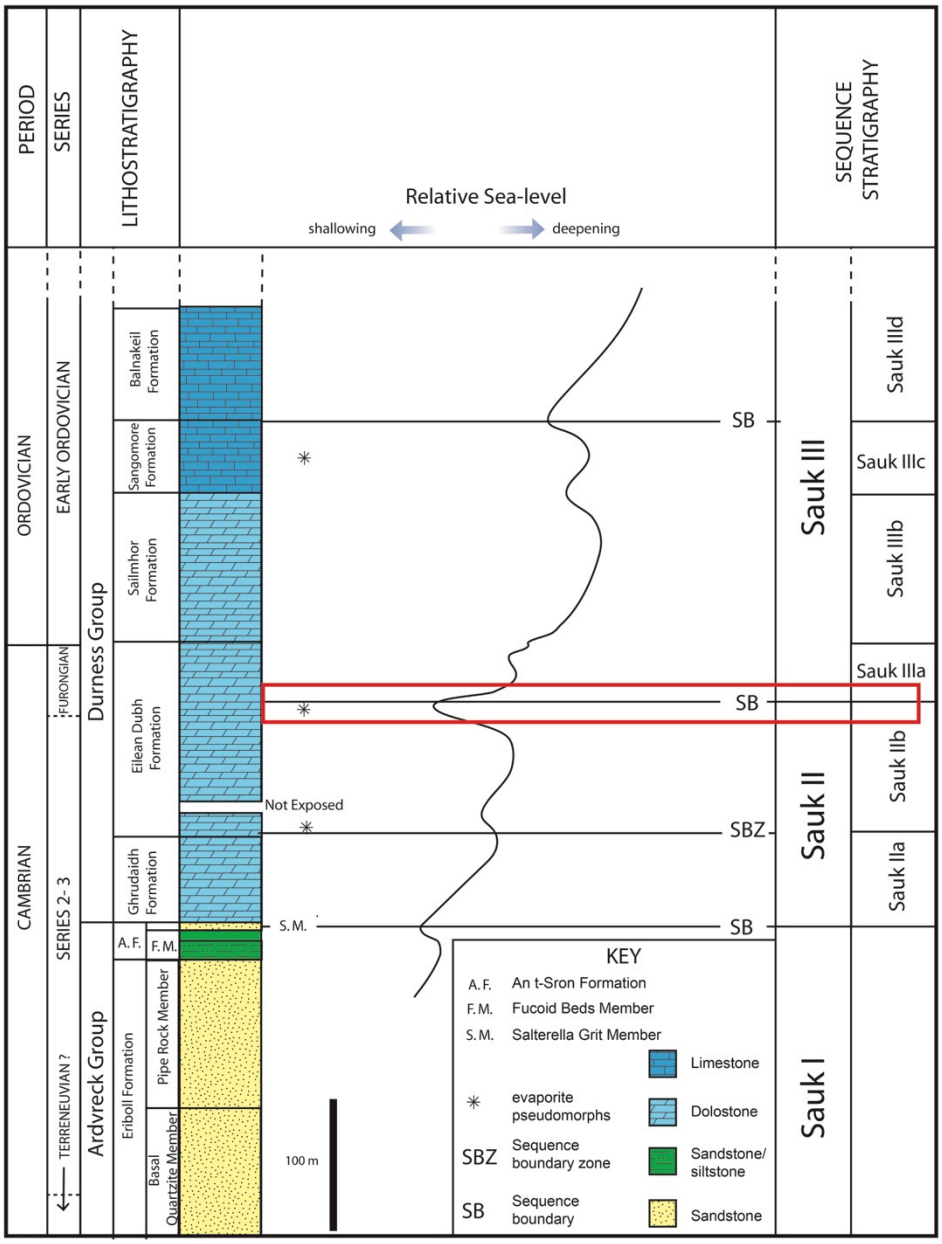

1650

Figure 3

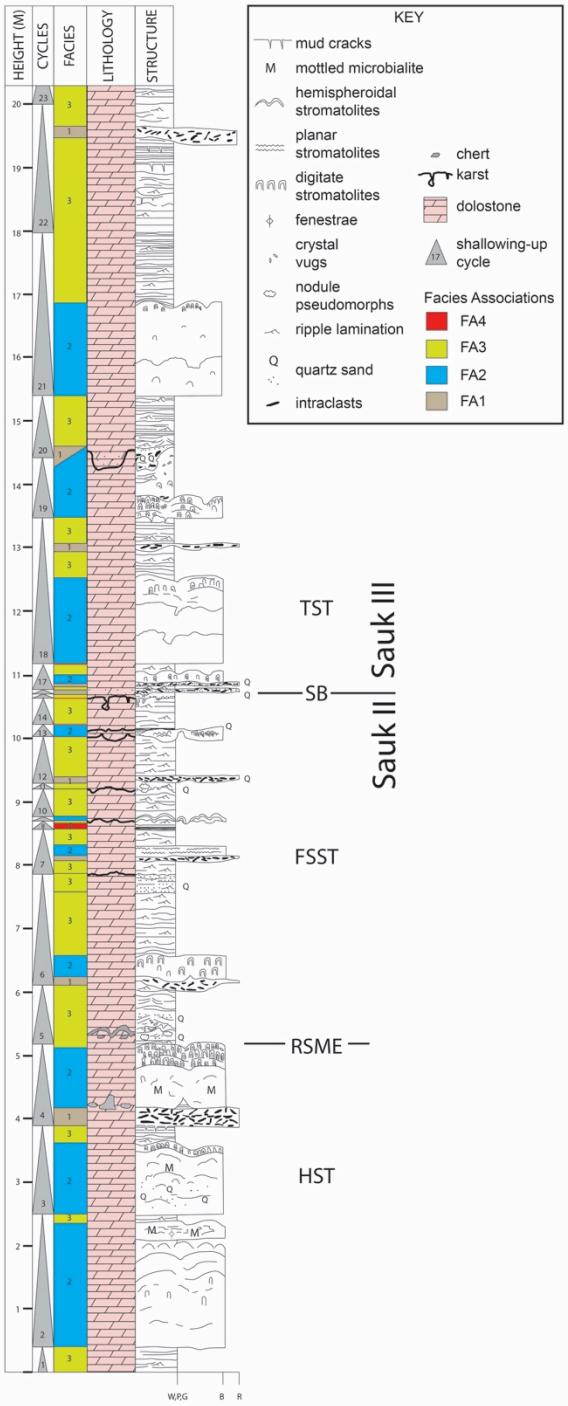

1651

Figure 4

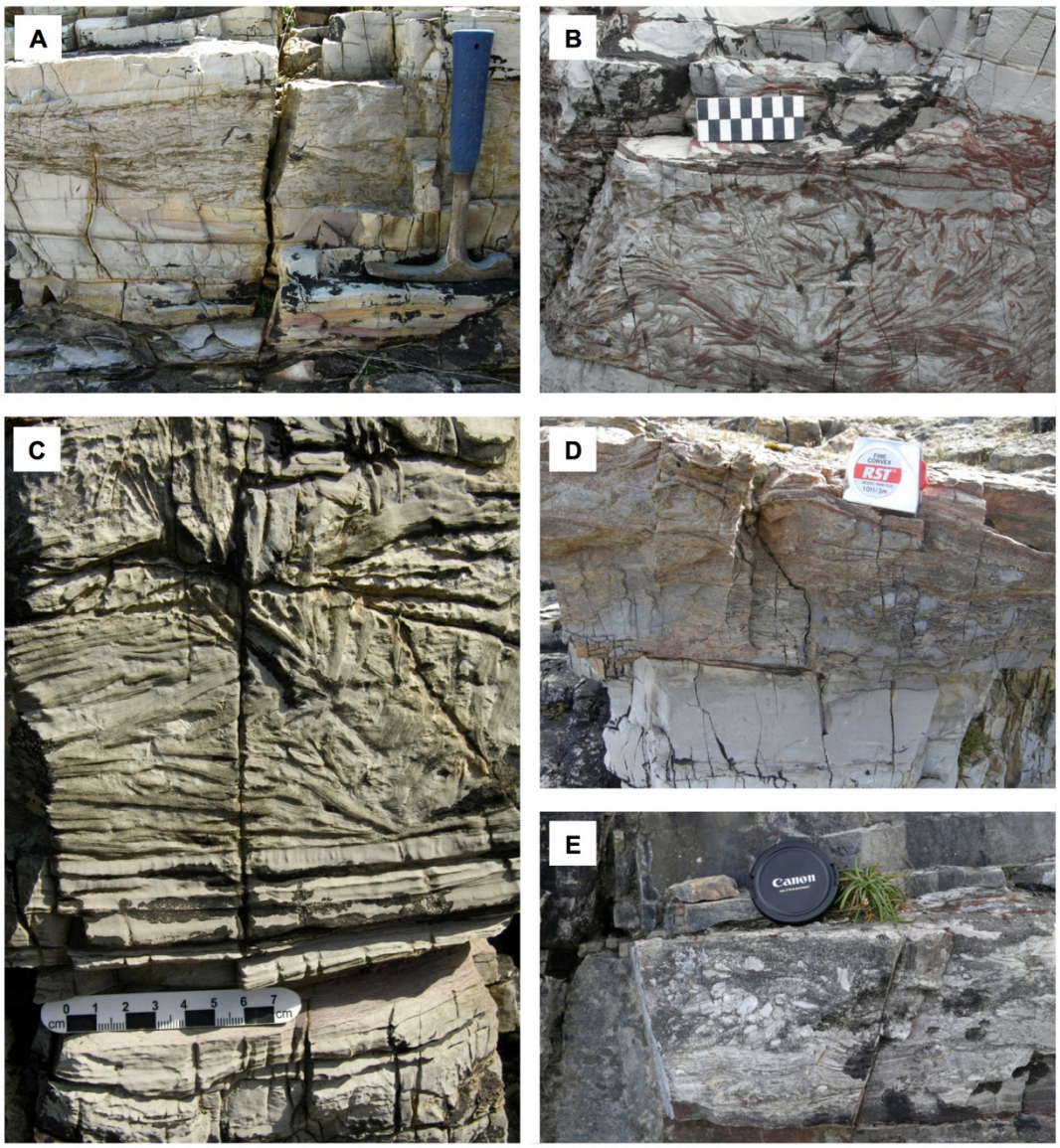

1652

Figure 5

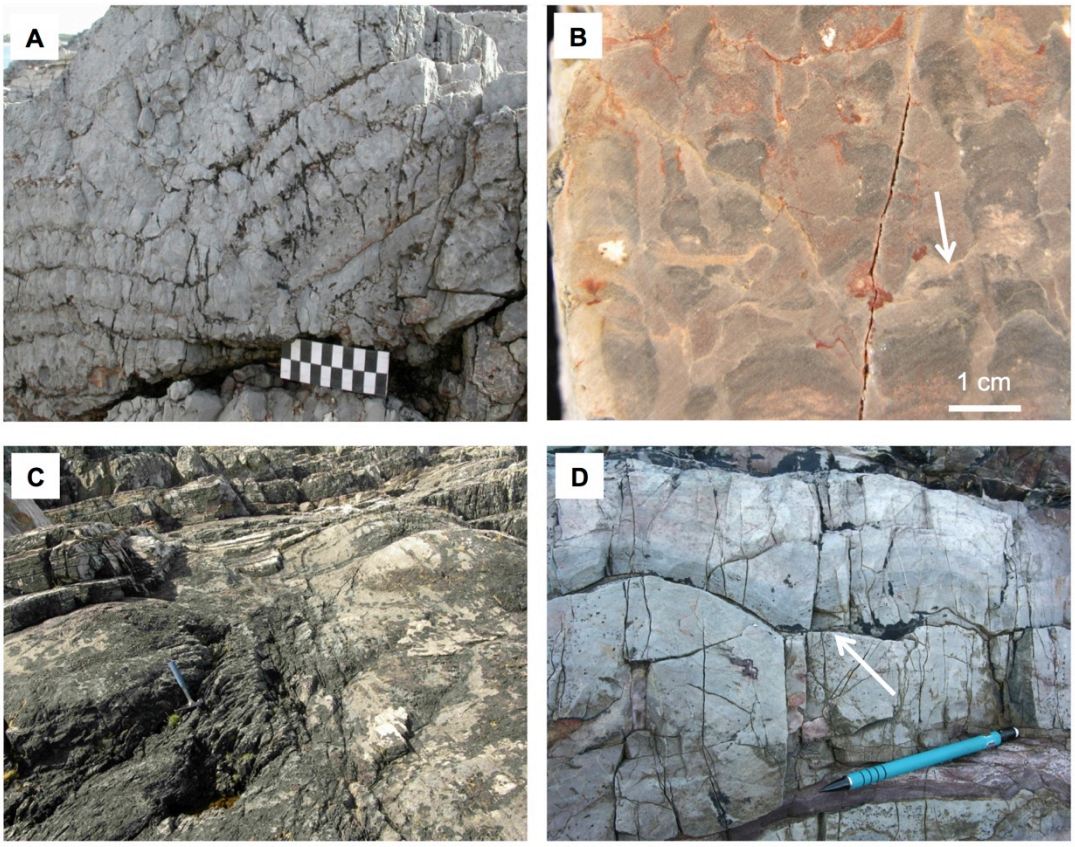

1653

Figure 6

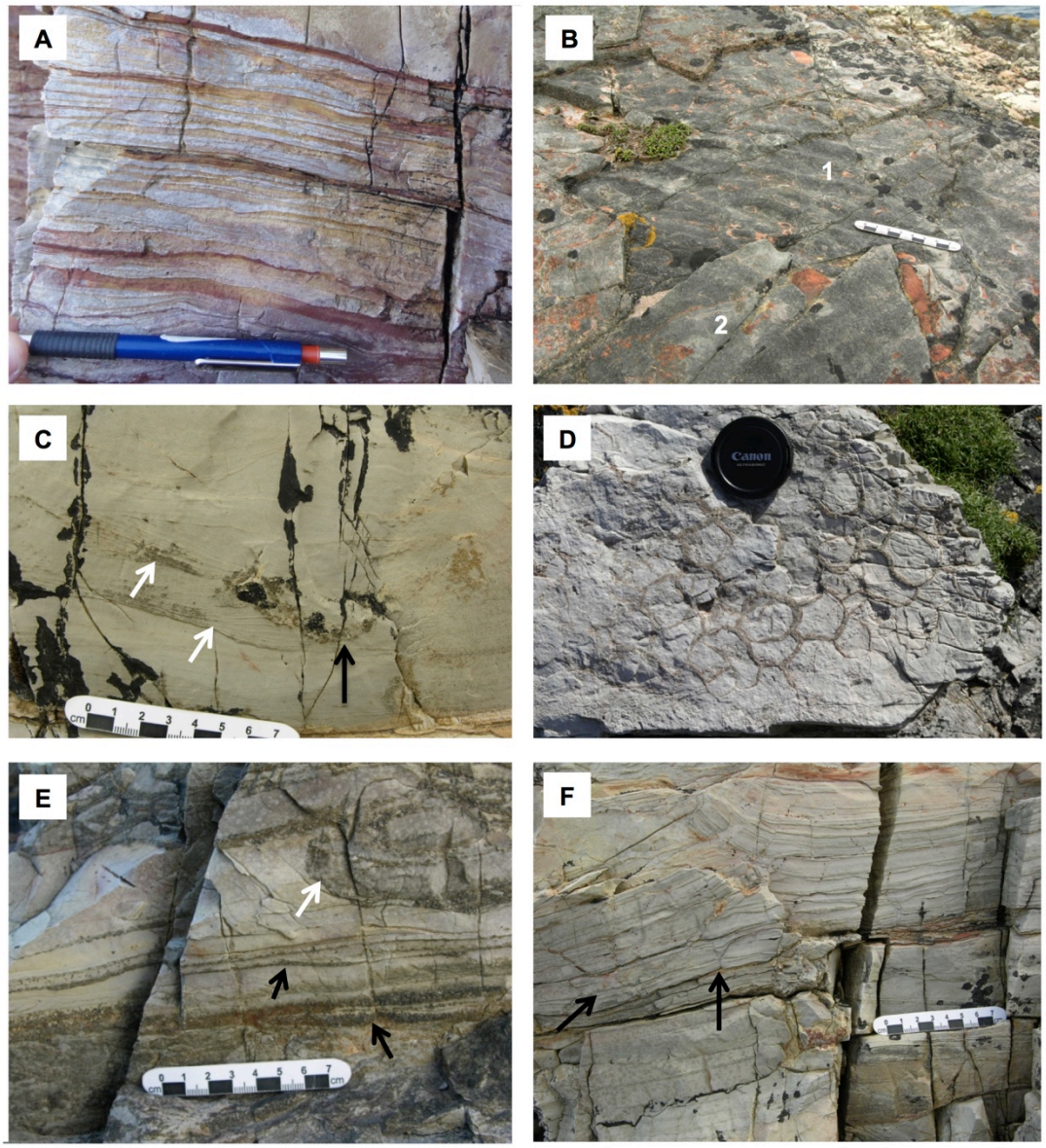

1654

Figure 7

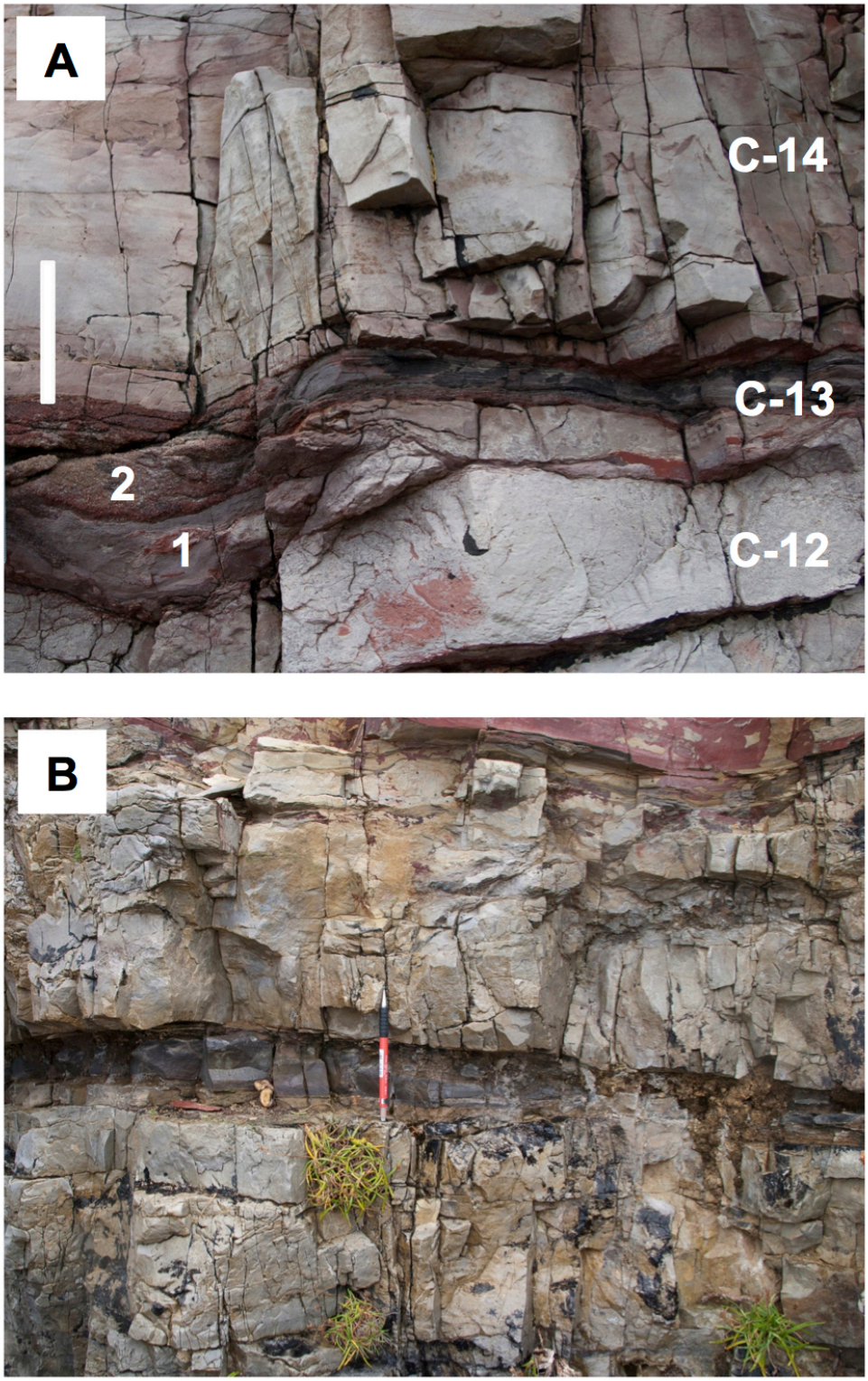

Figure 8

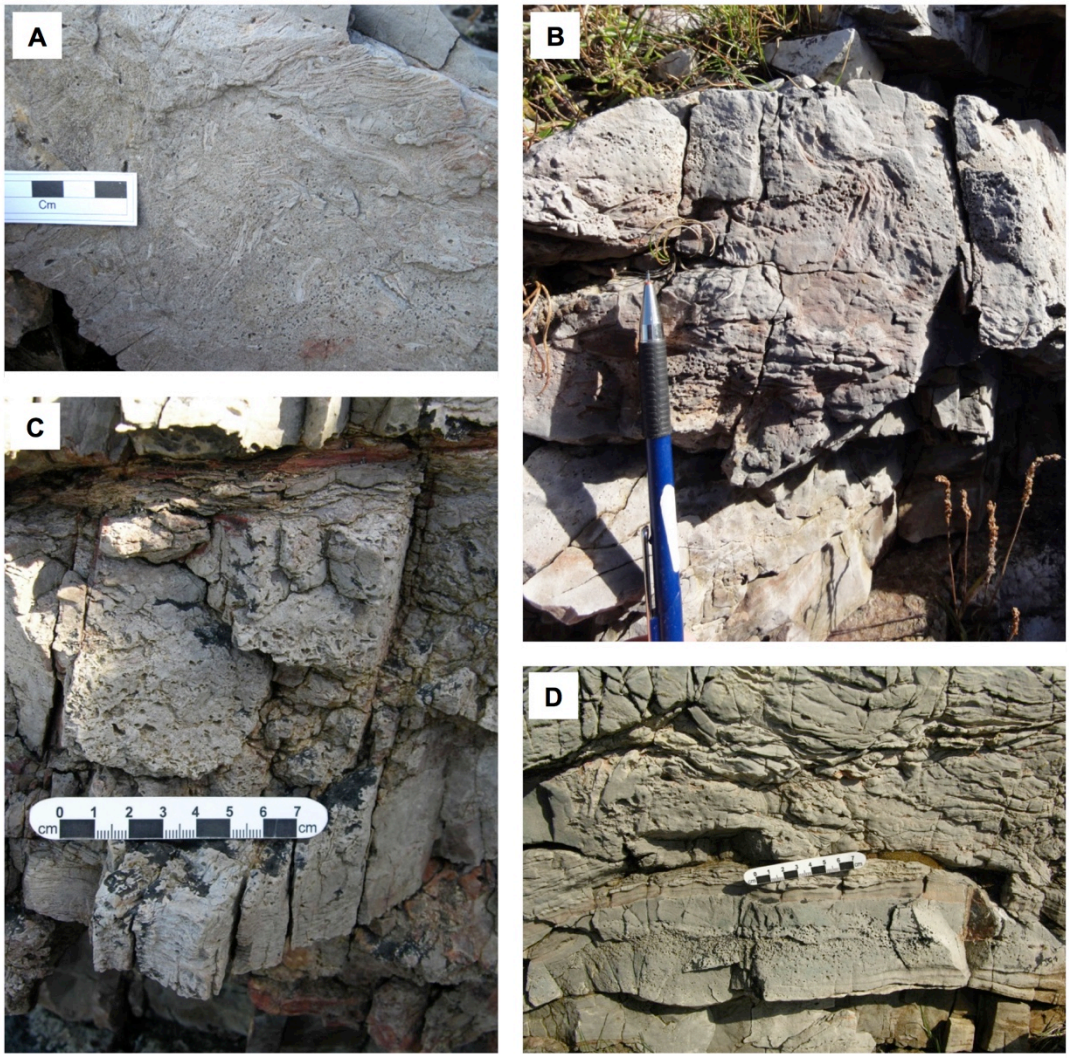

1656

Figure 9

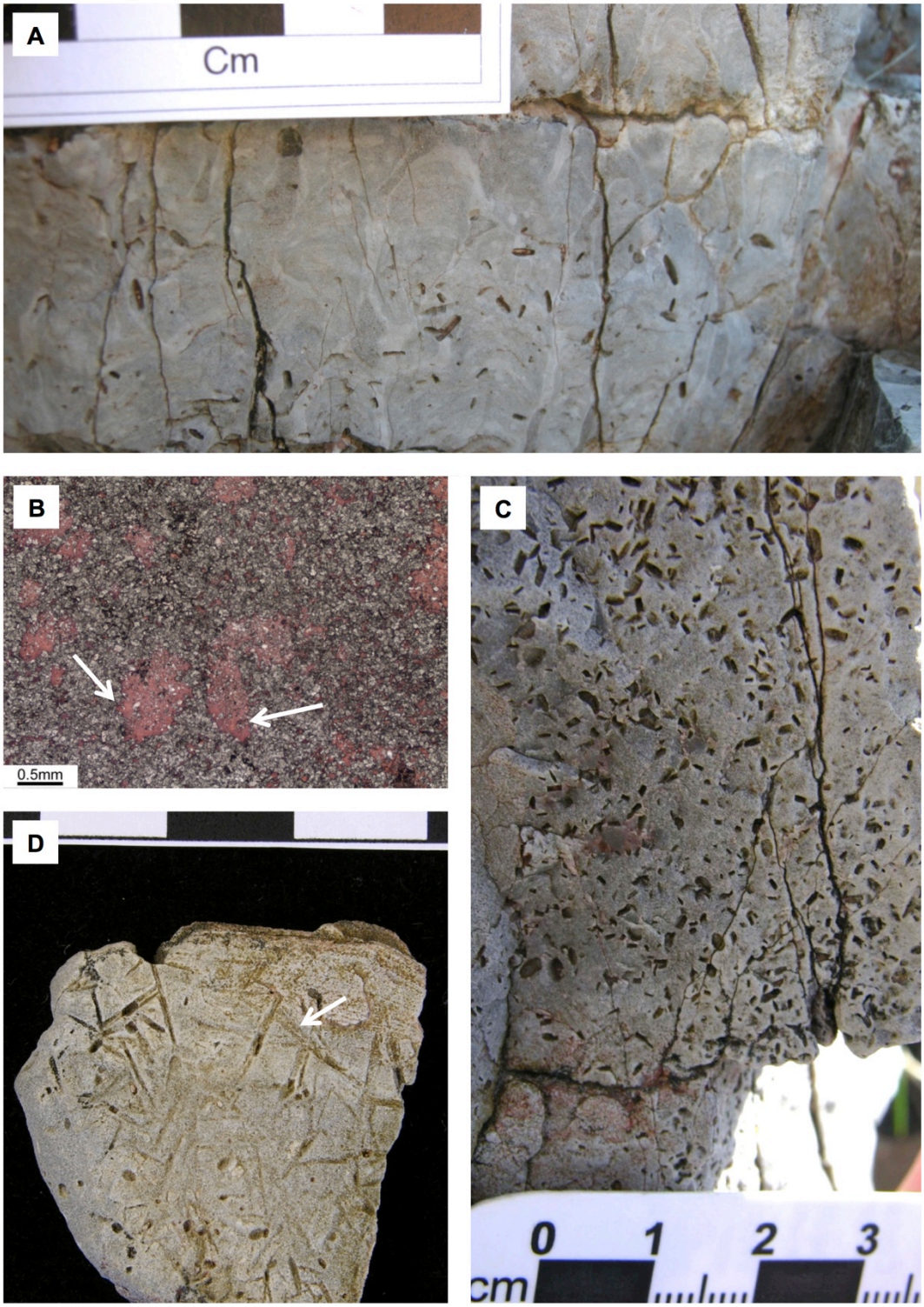

1657

Figure 10

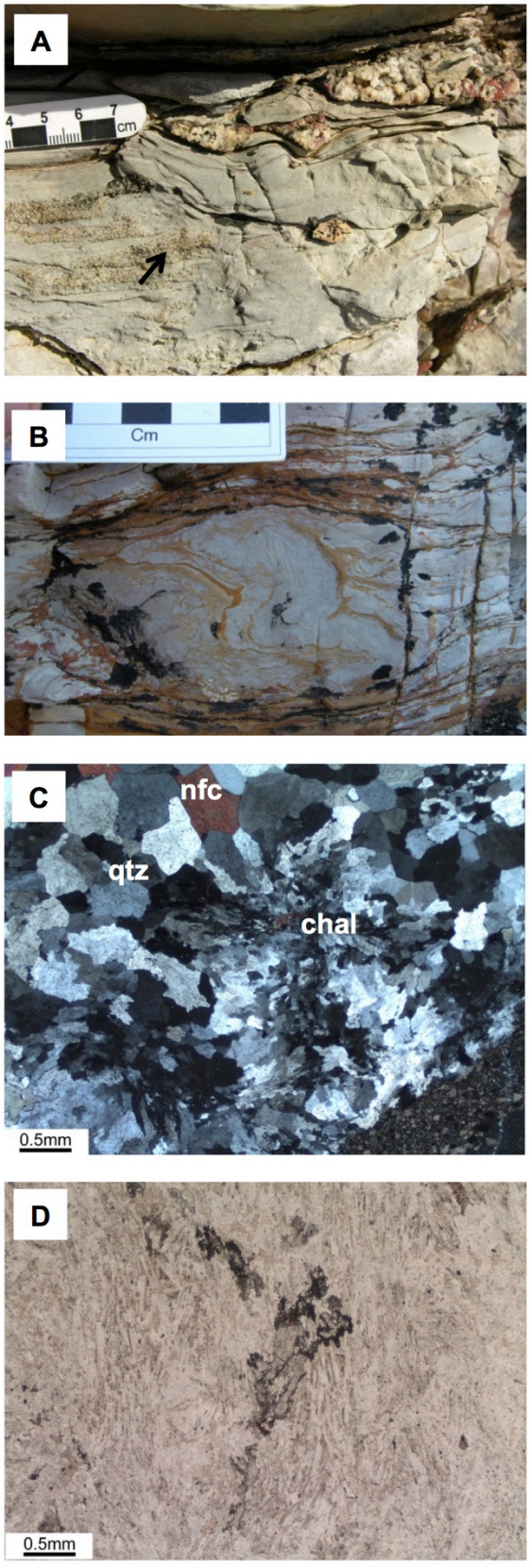

Figure 11

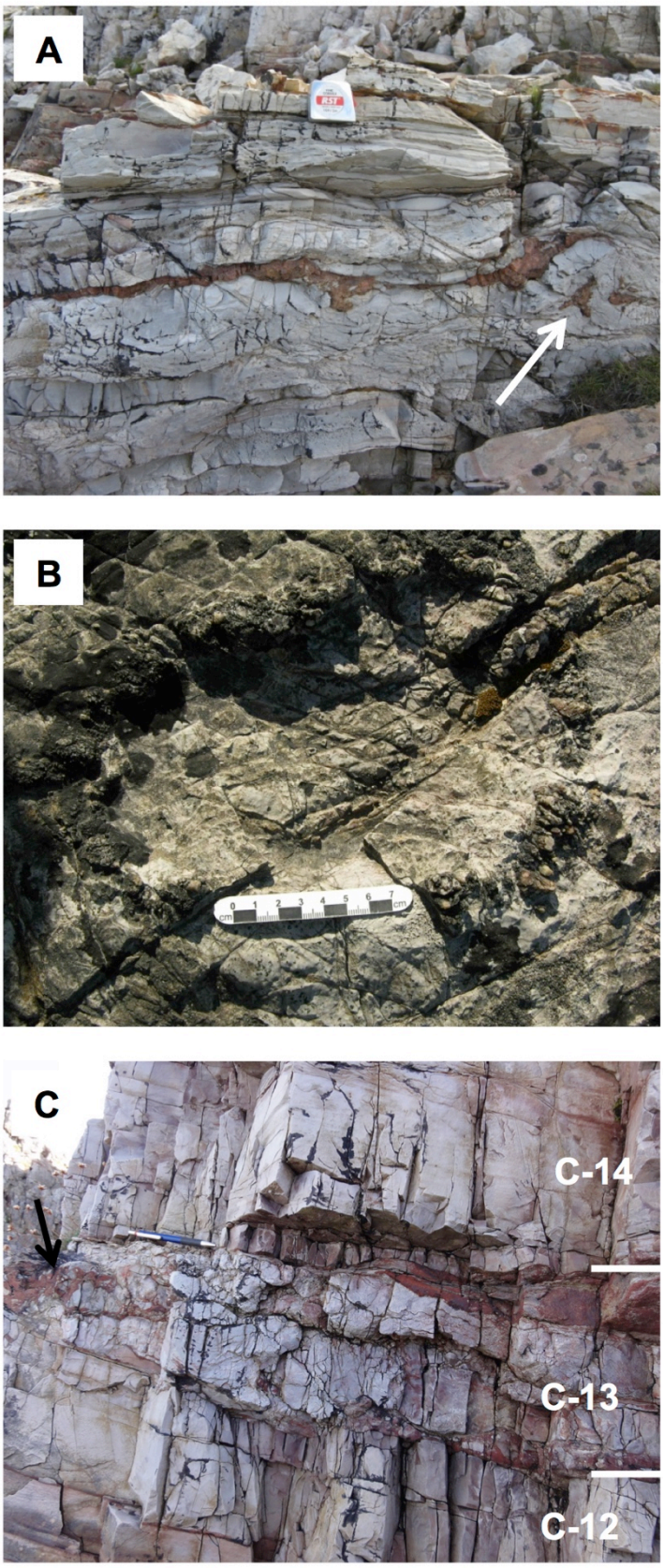

Figure 12

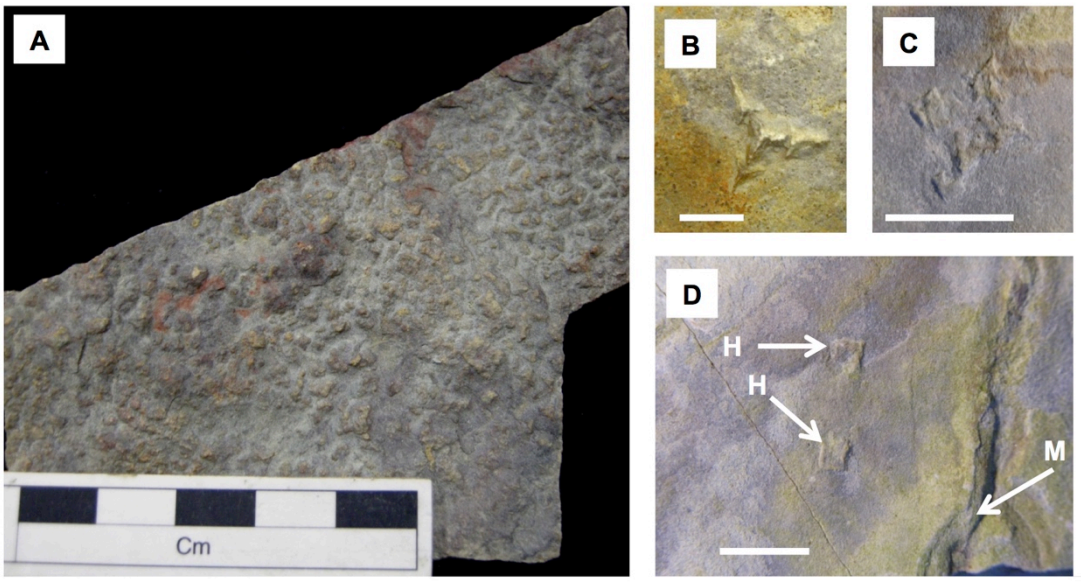

1660

Figure 13

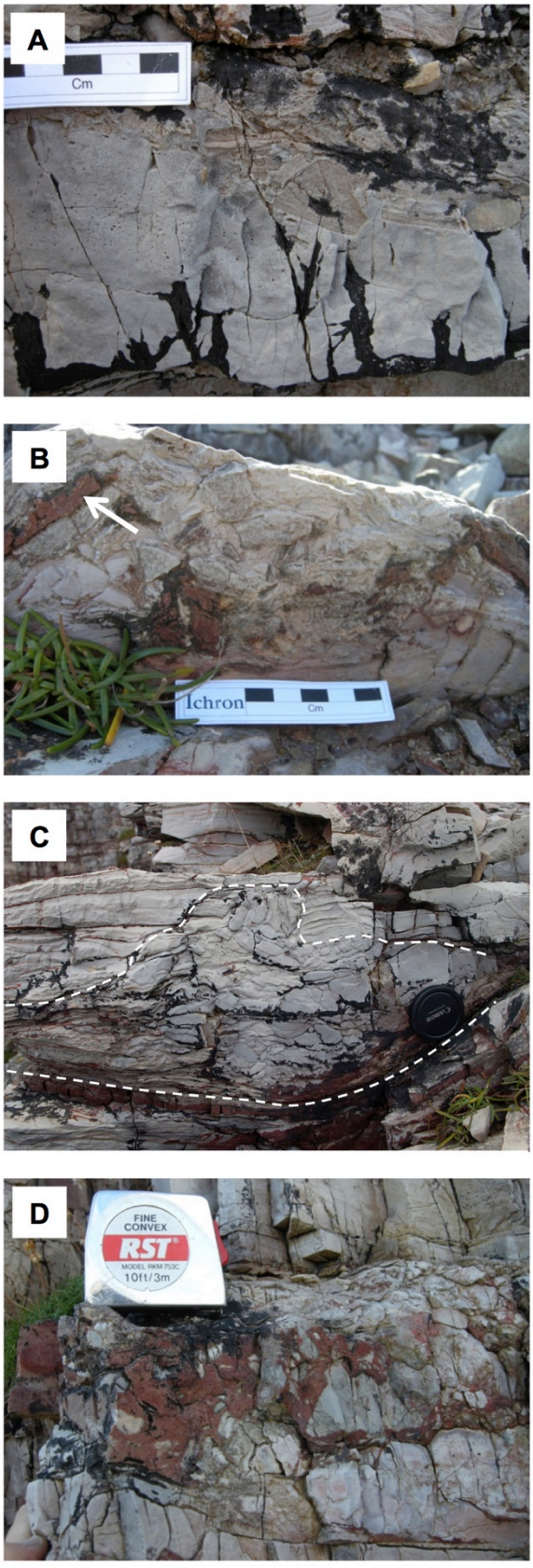

Figure 14

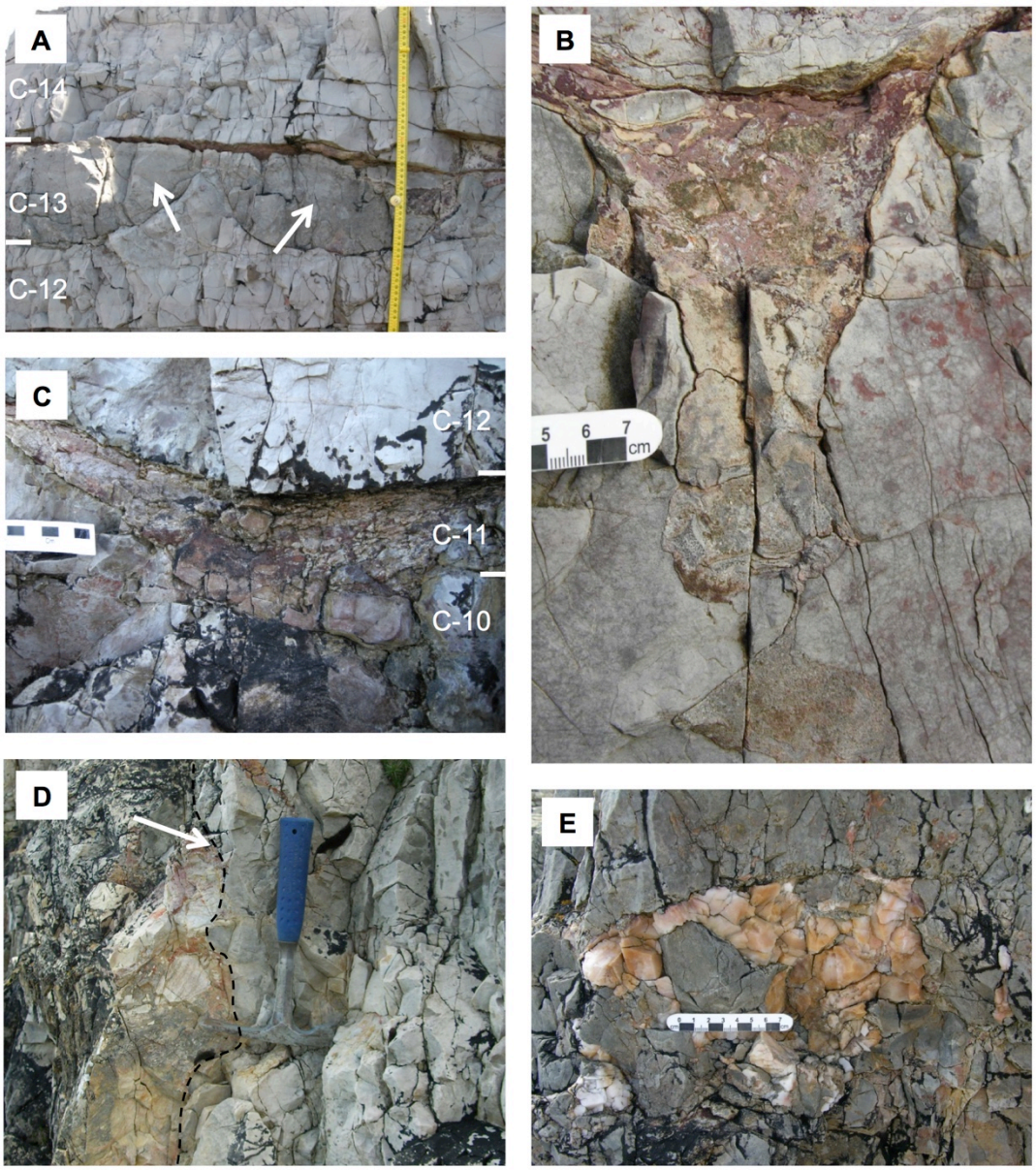

1662

Figure 15

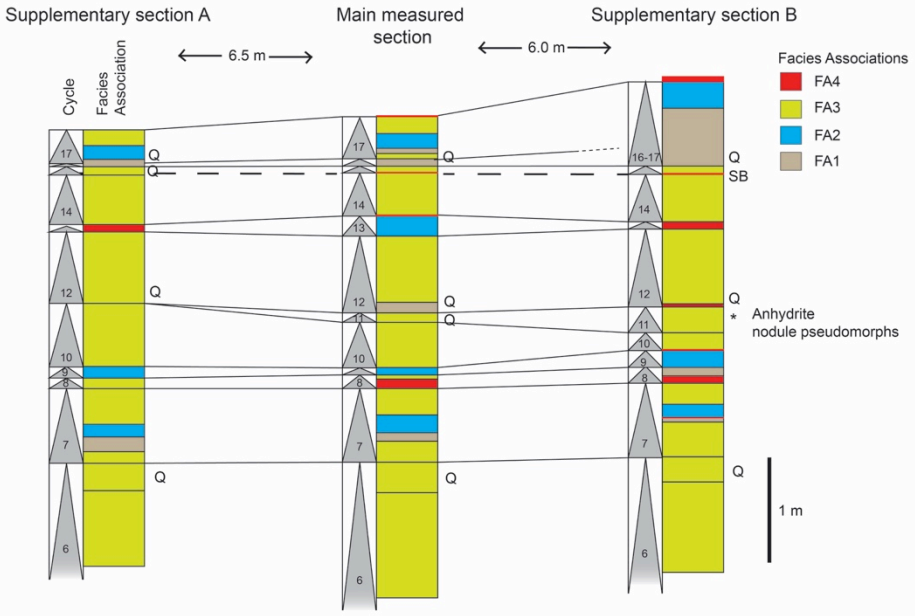

1663